10 Fluorescence Anisotropy

Measurements of fluorescence anisotropy are a powerful tool in biochemical research and medical testing. Upon excitation with polarized light the emission from many samples is also polarized. The extent of polarization of the emission is described in terms of the anisotropy (r). Samples exhibiting nonzero anisotropies are said to display polarized emission. The origin of anisotropy is the existence of transition moments for absorption and emission that lie along specific directions within the fluorophore structure. In homogeneous solution the ground-state fluorophores are all randomly oriented. When exposed to polarized light, those fluorophores that have their absorption transition moments oriented along the electric vector of the incident light are preferentially excited. Hence the excited-state population is partially oriented. A significant fraction of the excited molecules have their transition moments oriented along the electric vector of the polarized exciting light.

The emission can become depolarized by a number of processes, the relative importance of which depends upon the sample under investigation. All chromophores have transition moments that occur along a specific direction in the molecular axis. Rotational diffusion changes the direction of the transition moments and is one common cause of depolarization. Anisotropy measurements reveal the average angular displacement of the fluorophore that occurs between absorption and subsequent emission of a photon. This angular displacement is dependent upon the rate and extent of rotational diffusion during the lifetime of the excited state. The rate of rotational diffusion depends on the viscosity of the solvent and the size and shape of the rotating molecule. The rotational rate of fluorophores in solution is dependent upon the viscous drag imposed by the solvent. A change in solvent viscosity will result in a change in fluorescence anisotropy. For small fluorophores in low-viscosity solutions the rate of rotational diffusion is typically faster than the rate of emission. Under these conditions the emission is depolarized and the anisotropy close to zero.

The dependence of fluorescence anisotropy upon fluorophore motions has resulted in numerous applications of this technique in biochemical research. This is because the timescale of rotational diffusion of biomolecules is comparable to the decay time of many fluorophores. For instance, a protein with a molecular weight of 25 kD can be expected to have a rotational correlation time near 10 ns. This is comparable to the lifetime of many fluorophores. Hence factors that alter the rotational correlation time will also alter the anisotropy. For biomolecules the anisotropy is decreased due to both rotational diffusion and internal flexibility. As examples we note that fluorescence anisotropy measurements have been used to quantify protein denaturation, which usually results in increased flexibility of the peptide backbone, and protein association with other macromolecules, which changes the overall rate of rotation. Anisotropy measurements can also be used to measure the dynamics of proteins. The anisotropies of membrane-bound fluorophores have been used to estimate the internal viscosities of membranes and the effects of lipid composition upon the membrane phase-transition temperature. In addition, anisotropy measurements are widely used in clinical chemistry in the form of fluorescence-polarization immunoassays.

In this chapter we describe the fundamental theory for steady-state measurements of fluorescence anisotropy. We also describe selected biochemical applications. In the subsequent chapters we will describe time-resolved anisotropy measurements and advanced applications.

10.1. DEFINITION OF FLUORESCENCE ANISOTROPY

The measurement of fluorescence anisotropy is illustrated in Figure 10.1. For most experiments the sample is excited with vertically polarized light. The electric vector of the excitation light is oriented parallel to the vertical or z-axis. The intensity of the emission is measured through a polar-

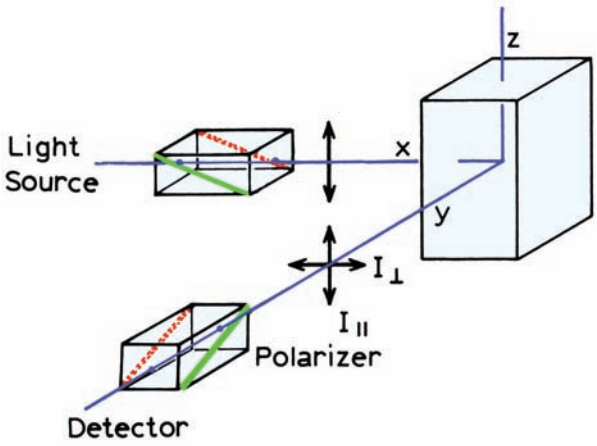

Figure 10.1. Schematic diagram for measurement of fluorescence anisotropies.

izer. When the emission polarizer is oriented parallel (||) to the direction of the polarized excitation the observed intensity is called $I_{\|}$. Likewise, when the polarizer is perpendicular ($\perp$) to the excitation the intensity is called $I_{\perp}$. These intensity values are used to calculate the anisotropy:[1]

$$r = \frac{I_{\|} - I_{\perp}}{I_{\|} + 2I_{\perp}} \tag{10.1}$$

The anisotropy is a dimensionless quantity that is independent of the total intensity of the sample. This is because the difference ($I_{\|} - I_{\perp}$) is normalized by the total intensity, which is $I_T = I_{\|} + 2I_{\perp}$. The anisotropy is an intensity ratiometric measurement. In the absence of artifacts the anisotropy is independent of the fluorophore concentration.

In earlier publications and in the clinical literature, the term polarization is frequently used. The polarization is given by

$$P = \frac{I_{\|} - I_{\perp}}{I_{\|} + I_{\perp}} \tag{10.2}$$

The polarization and anisotropy values can be interchanged using

$$P = \frac{3r}{2 + r} \tag{10.3}$$

$$r = \frac{2P}{3 - P} \tag{10.4}$$

The polarization and anisotropy contain the same information, but the use of polarization should be discouraged. Anisotropy is preferred because it is normalized by the total intensity $I_T = I_{\|} + 2I_{\perp}$, which results in simplification of the equations. Suppose the sample contains several emitting species with polarization values P_i and fractional intensities f_i. The polarization of this mixture (P) is given by[2]

$$\left(\frac{1}{P} - \frac{1}{3}\right)^{-1} = \sum_i \frac{f_i}{\left(\frac{1}{P_i} - \frac{1}{3}\right)} \tag{10.5}$$

In contrast, the average anisotropy ($\bar{r}$) is given by

$$\bar{r} = \sum_i f_i r_i \tag{10.6}$$

where r_i indicates the anisotropies of the individual species. The latter expression is clearly preferable. Furthermore, following pulsed excitation the fluorescence anisotropy decay $r(t)$ of a sphere is given by

$$r(t) = r_0 e^{-t/\theta} \tag{10.7}$$

where r_0 is the anisotropy at $t = 0$, and θ is the rotational correlation time of the sphere. The decay of polarization is not a single exponential, even for a spherical molecule.

Suppose that the light observed through the emission polarizer is completely polarized along the transmission direction of the polarizer. Then $I_{\perp} = 0$, and $P = r = 1.0$. This value can be observed for scattered light from an optically dilute scatterer. Completely polarized emission is never observed for fluorescence from homogeneous unoriented samples. The measured values are smaller due to the angular dependence of photoselection (Section 10.2.1). Completely polarized emission can be observed for oriented samples.

Now suppose the emission is completely depolarized. In this case $I_{\|} = I_{\perp}$ and $P = r = 0$. It is important to note that P and r are not equal for intermediate values. For the moment we have assumed these intensities could be measured without interference due to the polarizing properties of the optical components, especially the emission monochromator (Chapter 2). In Section 10.4 we will describe methods to correct for this effect.

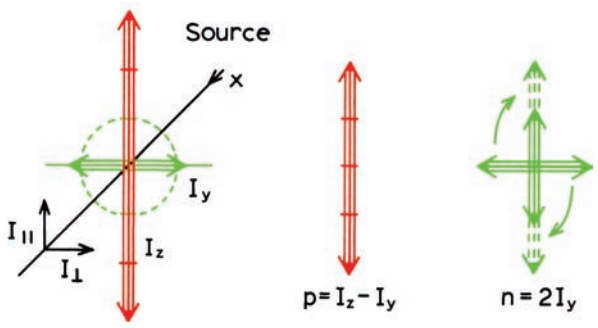

Figure 10.2. Polarization of a ray of light.

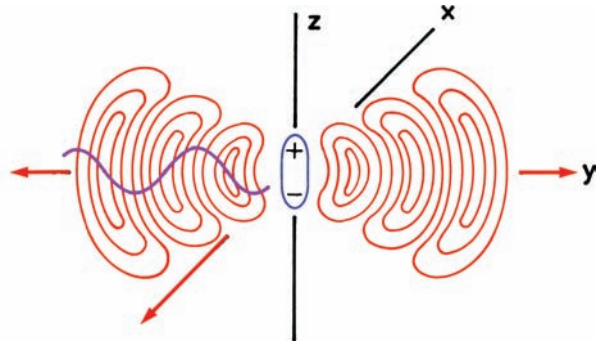

Figure 10.3. Electric field from a radiating dipole oriented along the *z*-axis. The thin arrows on the lines indicate the direction of the electric field *E*. The wide arrows indicate the direction of energy migration, which is symmetrical around the *z*-axis.

10.1.1. Origin of the Definitions of Polarization and Anisotropy

One may wonder why two widely used measures exist for the same phenomenon. Both P and r have a rational origin. Consider partially polarized light traveling along the x axis (Figure 10.2). The intensities I_z and I_y can be measured with a detector and polarizer positioned on the x-axis. The polarization of this light is defined as the fraction of the light that is linearly polarized. Specifically,

$$P = \frac{p}{p + n} \tag{10.8}$$

where p is the intensity of the polarized component and n the intensity of the natural component. The intensity of the natural component (n) is given by $n = 2I_y$. The remaining intensity is the polarized component, which is $p = I_z - I_y$. For vertically polarized excitation $I_z = I_{||}$ and $I_y = I_\perp$. Substitution into eq. 10.8 yields eq. 10.2, which is the standard definition for polarization.

The anisotropy (r) of a light source is defined as the ratio of the polarized component to the total intensity (I_T):

$$r = \frac{I_z - I_y}{I_x + I_y + I_z} = \frac{I_z - I_y}{I_T} \tag{10.9}$$

When the excitation is polarized along the z-axis, emission from the fluorophores is symmetric around the z-axis (Figure 10.3). Hence $I_x = I_y$. Recalling $I_y = I_\perp$ and $I_z = I_{||}$, one obtains eq. 10.1.

The polarization is an appropriate parameter for describing a light source when a light ray is directed along a particular axis. In this case $p + n$ is the total intensity and P the ratio of the excess intensity along the z-axis divided by the total intensity. This distribution of the emission is shown in Figure 10.3 for a dipole oriented along the z-axis. In contrast, the radiation emitted by a fluorophore is symmetrically distributed about the z-axis. The anisotropy is the ratio of the excess intensity that is parallel to the z-axis, divided by the total intensity. It is interesting to notice that a dipole oriented along the z-axis does not radiate along this axis, and cannot be observed with a detector on the z-axis.

10.2. THEORY FOR ANISOTROPY

The theory for fluorescence anisotropy can be derived by consideration of a single molecule.[3] Assume that the absorption and emission transition moments are parallel. This is nearly true for the membrane probe 1,6-diphenyl-1,3,5-hexatriene (DPH). Assume this single molecule is oriented with angles θ relative to the z-axis and ϕ relative to the y-axis (Figure 10.4). Of course, the ground-state DPH molecules will be randomly oriented in an isotropic solvent. If the excitation is polarized along the z-axis then there will be some preferential orientation of the excited-state population along this axis. It is known that emitting fluorophores behave like radiating dipoles.[4] Except for the quantized energy, the far-field radiation can be described completely by classical electrodynamics. Our goal is to calculate the anisotropy that would be observed for this oriented molecule in the absence of rotational diffusion. These assumptions of parallel dipoles, immobility, random ground-state orientation, and z-axis symmetry simplify the calculations.

Prior to deriving the expressions for anisotropy it is instructive to understand the origin of Figure 10.4. This figure shows $I_{||}$ and $I_\perp$ being proportional to the projection of the transition moment onto the axes. This is true because the projection of the transition moment is the same as the

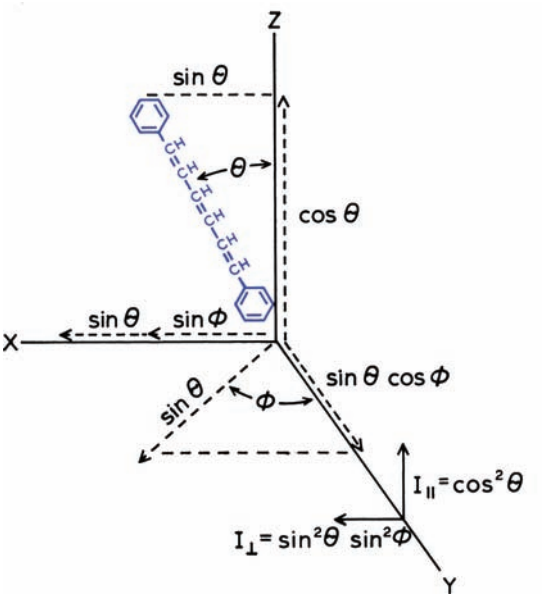

Figure 10.4. Emission intensities for a single fluorophore in a coordinate system.

projection of the electric field created by the fluorophore. The shape in Figure 10.3 shows the spatial distribution of light emitted by a dipole oriented along the z-axis. The electric field created by the fluorophore is described by[5–6]

$$E(\theta,\phi) = k\frac{\sin\theta}{r}\hat{\theta} \qquad (10.10)$$

where k is a constant, r is the distance from the fluorophore and $\hat{\theta}$ is a unit vector along the θ coordinate. The intensity of emitted light is proportional to the square of the electric field and is given by

$$I(\theta,\phi) = k^2\frac{\sin^2\theta}{r^2}\hat{r} \qquad (10.11)$$

where $\hat{r}$ is a unit vector in the direction of propagation.

With this background we can understand the parallel and perpendicular intensities due to a dipole with some arbitrary orientation. Figure 10.5 shows the emission intensity for a dipole oriented the same as the previous DPH molecule. The electric field is always tangential to this surface. Around the equator of this surface the electric field points in the same direction as the emission transition moment. Hence the projection of the field onto the z-axis is proportional to cos θ and the intensity is proportional to

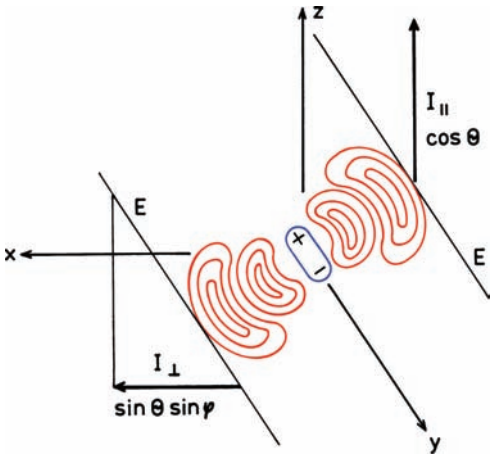

Figure 10.5. Radiating dipole in a coordinate system.

$\cos^2\theta$. Similarly, the field along the x-axis is proportional to sin θ sin ϕ. The polarized intensities are due to the projected electric fields, but it is usually easier to think in terms of molecular orientation rather than the radiated field. Hence we use diagrams such as Figure 10.4 to describe the anisotropy theory.

We now know the light polarized intensity along an axis is proportional to projection of the transition moments into this axis. Hence the parallel and perpendicular intensities for the molecule in Figure 10.4 are given by

$$I_{\|}(\theta,\phi) = \cos^2\theta \qquad (10.12)$$

$$I_{\perp}(\theta,\phi) = \sin^2\theta\sin^2\phi \qquad (10.13)$$

We now need to consider randomly oriented fluorophores excited with polarized light. The anisotropy is calculated by performing the appropriate averaged intensities based on excitation photoselection and how the selected molecules contribute to the measured intensity. For excitation polarized along the z-axis all molecules at an angle ϕ from the y-axis are excited with equal probability. That is, the population of excited fluorophore is symmetrically distributed around the z-axis. The population of excited molecules is oriented with values of ϕ from 0 to 2π with equal probability. Hence we can eliminate the ϕ dependence in eq. 10.13. The average value of $\sin^2\phi$ is given by

$$<\sin^2\phi> = \frac{\int_0^{2\pi}\sin^2\phi\,d\phi}{\int_0^{2\pi}d\phi} = \frac{1}{2} \qquad (10.14)$$

and therefore

$$I_{\|}(\theta) = \cos^2\theta \tag{10.15}$$

$$I_{\perp}(\theta) = \frac{1}{2}\sin^2\theta \tag{10.16}$$

Now assume we are observing a collection of fluorophores that are oriented relative to the z-axis with a probability $f(\theta)$. In the following section we will consider the form of $f(\theta)$ expected for excitation photoselection. The measured fluorescence intensities for this collection of molecules are

$$I_{\|} = \int_0^{\pi/2} f(\theta)\cos^2\theta\, d\theta = k\langle\cos^2\theta\rangle \tag{10.17}$$

$$I_{\perp} = \frac{1}{2}\int_0^{\pi/2} f(\theta)\sin^2\theta\, d\theta = \frac{k}{2}\langle\sin^2\theta\rangle \tag{10.18}$$

where $f(\theta)\,d\theta$ is the probability that a fluorophore is oriented between θ and $\theta + d\theta$, and k is an instrumental constant. Using eq. 10.1 and the identity $\sin^2\theta = 1 - \cos^2\theta$, one finds that

$$r = \frac{3\langle\cos^2\theta\rangle - 1}{2} \tag{10.19}$$

Hence the anisotropy is determined by the average value of $\cos^2\theta$, where θ is the angle of the emission dipole relative to the z-axis. This expression is only correct for samples that display z-axis symmetry. A different expression is needed to describe the anisotropy of a fluorophore oriented with unique angles θ and ϕ.

It is instructive to consider the relationship between r and θ. For a single fluorophore oriented along the z-axis, with colinear transitions, $\theta = 0$, the use of eq. 10.19 shows that $r = 1.0$. However, it is not possible to obtain a perfectly oriented excited-state population with optical excitation of homogeneous solutions. Hence the anisotropies are always less than 1.0. Complete loss of anisotropy is equivalent to $\theta = 54.7°$. This does not mean that each fluorophore is oriented at 54.7°, or that they have rotated through 54.7°. Rather, it means that the average value of $\cos^2\theta$ is 1/3, where θ is the angular displacement between the excitation and emission moments. In the derivation of eq. 10.19 we assumed that the transition moments were colinear. A slightly more complex expression is necessary for almost all fluorophores because the transition moments are rarely colinear. In addition, we have not yet considered the effects of photoselection on the anisotropy values.

10.2.1. Excitation Photoselection of Fluorophores

When a sample is illuminated with polarized light, those molecules with absorption transitions aligned parallel to the electric vector of the polarized excitation have the highest probability of excitation. The electric dipole of a fluorophore need not be precisely aligned with the z-axis to absorb light polarized among this axis. The probability of absorption is proportional to the $\cos^2\theta$, where θ is the angle the absorption dipole makes with the z-axis.[7] Hence, excitation with polarized light results in a population of excited fluorophores that are partially oriented along the z-axis (Figure 10.6). This phenomenon is called photoselection. The excited-state population is symmetrical around the z-axis. Most of the excited fluorophores are aligned close to the z-axis, and very few fluorophores have their transition moments oriented in the x-y plane. For the random ground-state distribution, which must exist in a disordered solution, the number of molecules at an angle between θ and $\theta + d\theta$ is proportional to $\sin\theta\, d\theta$. This quantity is proportional to the surface area on a sphere within the angles θ and $\theta + d\theta$.

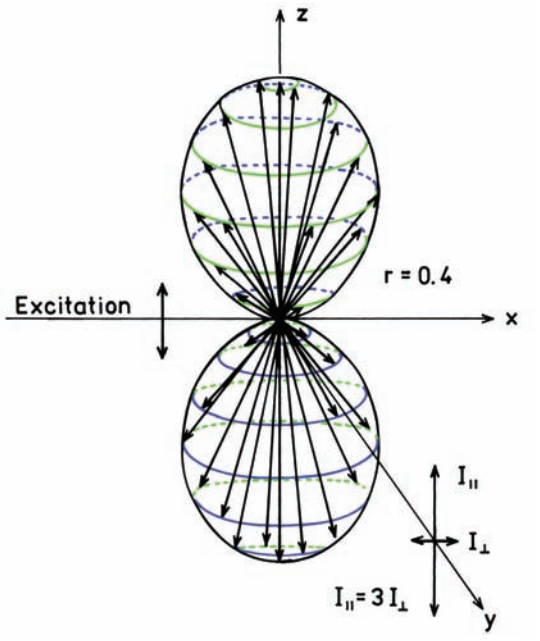

Figure 10.6. Excited-state distribution for immobile fluorophores with $r_0 = 0.4$.

Hence, the distribution of molecules excited by vertically polarized light is given by

$$f(\theta)\,d\theta = \cos^2\theta \sin d\theta \qquad (10.20)$$

The probability distribution given by eq. 10.20 determines the maximum photoselection that can be obtained using one-photon excitation of an isotropic solution. More highly oriented populations can be obtained using multiphoton excitation.[7]

The anisotropy is a function of $<\cos^2\theta>$ (eq. 10.19). Hence, calculation of $<\cos^2\theta>$ allows calculation of the anisotropy. For colinear absorption and emission dipoles the value of $<\cos^2\theta>$ is given by

$$<\cos^2\theta> = \frac{\int_0^{\pi/2}\cos^2\theta\ f(\theta)\ d\theta}{\int_0^{\pi/2} f(\theta)\,d\theta} \qquad (10.21)$$

Substitution of 10.20 into 10.21 yields $<\cos^2\theta> = 3/5$. Equation 10.19 shows a maximum anisotropy of 0.4. This is the value that is observed when the absorption and emission dipoles are colinear, and when there are no processes which result in depolarization. Under these conditions the excited-state population is preferentially oriented along the z-axis (Figure 10.6) and the value of $I_\perp$ is one-third the value of $I_\parallel$ ($I_\parallel = 3I_\perp$). This value of $r = 0.4$ is considerably smaller than that possible for a single fluorophore oriented along the z-axis ($r = 1.0$).

It is important to remember that there are other possible origins for polarized light. These include reflections and light scattered by the sample. For a dilute scattering solution, where there is a single scattering event, the anisotropy is close to 1.0. Scattered light can interfere with anisotropy measurements. If the measured anisotropy for a randomly oriented sample is greater than 0.4, one can confidently infer the presence of scattered light in addition to fluorescence. The maximum anisotropy of 0.4 for colinear absorption and emission dipoles is a consequence of the $\cos^2\theta$ probability of light absorption. Anisotropy values can exceed 0.4 for multiphoton excitation (Chapter 18).

10.3. EXCITATION ANISOTROPY SPECTRA

In the preceding section we assumed that the absorption and emission moments were colinear ($r_0 = 0.4$). Few fluorophores display $r_0 = 0.4$. For most fluorophores the r_0 values are less than 0.4, and in general the anisotropy values depend on the excitation wavelength. This is explained by the transition moments being displaced by an angle β relative to each other. In the previous section (eqs. 10.12–10.19) we demonstrated that displacement of the emission dipole by an angle θ from the z-axis resulted in a decrease in the anisotropy by a factor $(3\cos^2\theta - 1)/2$. Similarly, the displacement of the absorption and emission dipoles by an angle β results in a further loss of anisotropy. The observed anisotropy in a vitrified dilute solution is a product of the loss of anisotropy due to photoselection (2/5), and that due to the angular displacement of the dipoles. The fundamental anisotropy of a fluorophore is given by

$$r_0 = \frac{2}{5}\left(\frac{3\cos^2\beta - 1}{2}\right) \qquad (10.22)$$

where β is the angle between the absorption and emission transitions.

The term r_0 is used to refer to the anisotropy observed in the absence of other depolarizing processes such as rotational diffusion or energy transfer. For some molecules β is close to zero. For example, r_0 values as high as 0.39 have been measured for DPH, although slightly lower values are frequently reported.[8–10] An anisotropy of 0.39 corresponds to an angle of 7.4° between the dipoles, whereas $r_0 = 0.4$ corresponds to an angle of 0°. The fundamental anisotropy value is zero when β = 54.7°. When β exceeds 54.7° the anisotropy becomes negative. The maximum negative value (–0.20) is found for β = 90°. These values for both r_0 and P_0 are summarized in Table 10.1. For any fluorophore randomly distributed in solution, with one-photon excitation, the value of r_0 must be within the range from –0.20 to 0.40 for single-photon excitation.

Measurement of the fundamental anisotropy requires special conditions. In order to avoid rotational diffusion the probes are usually examined in solvents that form a clear glass at low temperature, such as propylene glycol or glyc-

Table 10.1. Relationship between the Angular Displacement of Transition Moments (β) and the Fundamental Anisotropy (r_0) or Polarization (P_0)

β (deg)	r_0	P_0
0	0.40	0.50 = 1/2
45	0.10	0.143 =1/7
54.7	0.00	0.000
90	–0.20	–0.333 = –1/3

erol. Additionally, the solutions must be optically dilute to avoid depolarization due to radiative reabsorption and emission, or due to resonance energy transfer. One commonly used solvent for measuring fundamental anisotropies is propylene glycol at –60 to –70°C. Under these conditions the fluorophores remain immobile during the lifetime of the excited state. Glycerol also forms a rigid glass at low temperature. However, glycerol typically displays more autofluorescence than propylene glycol. At similar temperatures phosphorescence from the fluorophores seems to be more common in glycerol than in propylene glycol. In these rigid solutions the measured anisotropy values (r_0) provide a measure of the angle between the absorption and emission dipoles (eq. 10.22). Since the orientation of the absorption dipole differs for each absorption band, the angle β varies with excitation wavelength. The changes in the fundamental anisotropy with excitation wavelength can be understood as a rotation of the absorption transition moment. A more precise explanation may be the changing contributions of two or more electronic transitions, each with a different value of β. As the excitation wavelength changes, so does the fraction of the light absorbed by each transition (Section 10.3.1).

The anisotropy spectrum is a plot of the anisotropy versus the excitation wavelength for a fluorophore in a dilute vitrified solution. The anisotropy is usually independent of the emission wavelength, so only excitation anisotropy spectra are reported. The lack of dependence on emission wavelength is expected since emission is almost always from the lowest singlet state. If emission occurs from more than one state, and if these states show different emission spectra, then the anisotropies can be dependent upon emission wavelength. Such dependence can also be observed in the presence of solvent relaxation (Chapter 7). In this case anisotropy decreases with increasing wavelength because the average lifetime is longer for longer wavelengths (Chapter 12). This effect is generally observed when the spectral relaxation time is comparable to the fluorescence lifetime. In completely vitrified solution, where solvent relaxation does not occur, the anisotropy is usually independent of emission wavelength.

The largest r_0 values are usually observed for excitation into the longest wavelength absorption band.[11] This is because the lowest singlet state is generally responsible for the observed fluorescence, and this state is also responsible for the long-wavelength absorption band (Kasha's rule). Absorption and emission involving the same electronic transition have nearly colinear moments. Larger β values

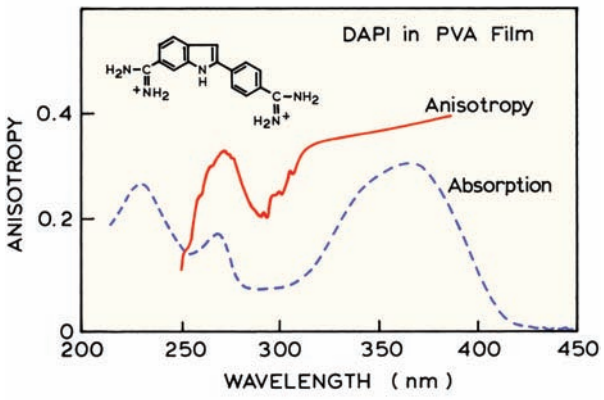

Figure 10.7. Excitation anisotropy spectra of DAPI in an unstretched polyvinyl alcohol film (solid). The dashed line is the absorption spectrum. Revised and reprinted with permission from [15]. Copyright © 1989, American Chemical Society.

(lower r_0 values) are obtained upon excitation into higher electronic states, which are generally not the states responsible for fluorescence emission. Rather, the fluorophores relax very rapidly to the lowest singlet state. The excitation anisotropy spectrum reveals the angle between the absorption and emission transition moments. However, the direction of these moments within the molecule itself are not revealed. Such a determination requires studies with ordered systems, such as crystals or stretched films.[12–14]

These general features of an anisotropy spectrum are illustrated in Figure 10.7 for DAPI in an isotropic (unstretched) polyvinyl alcohol film.[15] This film is very viscous, so the fluorophores cannot rotate during the excited-state lifetime. The absorption and emission dipoles are in the plane of the rings. For excitation wavelengths longer than 330 nm the r_0 value is relatively constant. The relatively constant r_0 value across the $S_0 \rightarrow S_1$ transition, and a gradual tendency towards higher r_0 values at longer wavelengths, is typical of many fluorophores. As the excitation wavelength is decreased the anisotropy becomes more strongly dependent on wavelength. Different anisotropies are expected for the $S_0 \rightarrow S_1$, $S_0 \rightarrow S_2$ and higher transitions.

The excitation anisotropy spectrum of DAPI is rather ideal because r_0 is relatively constant across the long wavelength absorption band. Many fluorophores show a gradual decrease in r_0 as the excitation wavelength is decreased. This property is illustrated for 9-anthroyloxy stearic acid (9-AS) in Figure 10.8. When using such probes careful control of the excitation wavelength is needed if the experiments depend on knowledge of the r_0 values.

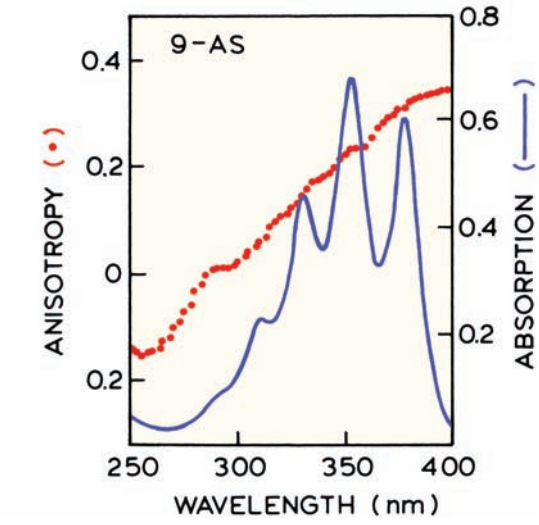

Figure 10.8. Excitation anisotropy spectrum of 9-anthroyloxy stearic acid (9-AS) in propylene glycol at –52°C. The same excitation anisotropy spectrum was observed for 2-AS, 7-AS, 12-AS and 16-AP. Revised and reprinted with permission from [16]. Copyright © 1982, American Chemical Society.

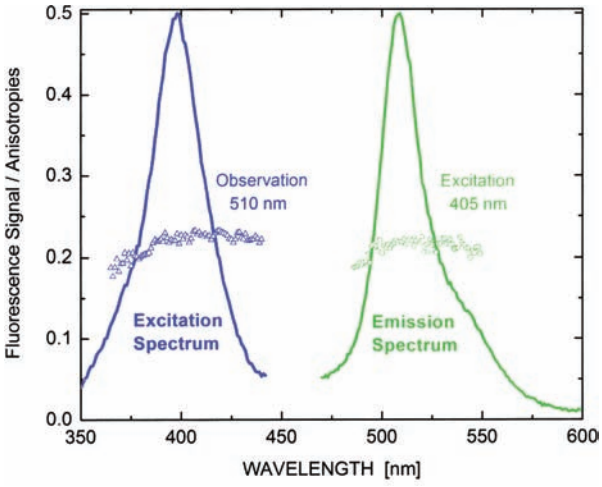

Figure 10.9. Excitation anisotropy spectrum of Green Fluorescent Protein. Figure courtesy of Drs. Z. Gryczynski, L. Black and R. B. Thompson.

Figure 10.9 shows excitation and emission anisotropy spectra for GFP that was packaged into the heads of T4 bacteriophage.[17] Each phage head contains about 90 GFP molecules. Given the size of the phage heads, the anisotropy is expected to be close to the fundamental anisotropy, which is near 0.38. Homotransfer between the concentrated GFP molecules was suggested as the reason for the lower

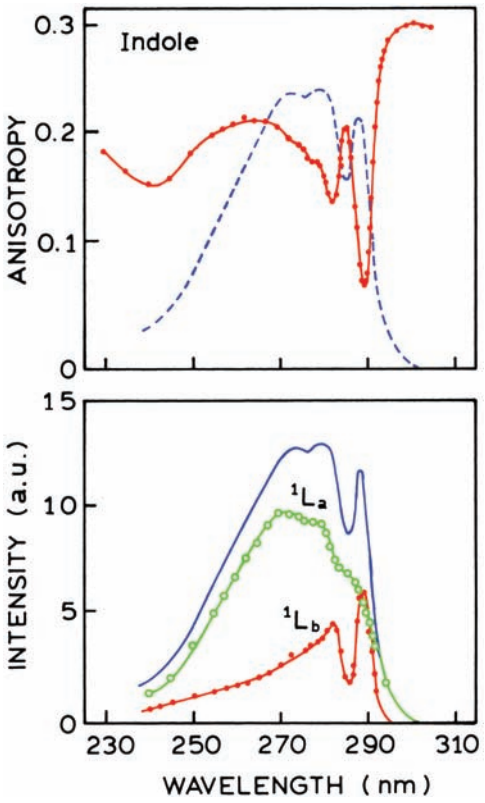

Figure 10.10. Excitation anisotropy spectrum of indole in vitrified propylene glycol. Also shown are the calculated absorption spectra of the ^1L_a and ^1L_b states. Revised from [19].

anisotropy. The anisotropy is constant across the emission spectrum, which is typical of emission anisotropy spectra.

10.3.1. Resolution of Electronic States from Polarization Spectra

Some fluorophores can display complex anisotropy spectra, even across the longest absorption band. One well-known example is indole.[18–20] The anisotropy varies abruptly with excitation wavelength across the long-wavelength absorption band (Figure 10.10, top). This dependence was attributed to the two excited states of indole (^1L_a and ^1L_b), which are responsible for the absorption from 250 to 300 nm.[21–22] The transition moments are thought to be at an angle of 90° relative to one another.[23–24] Emission of indole occurs mainly from the ^1L_a state.

This complex anisotropy spectrum can be used to determine the absorption spectra corresponding to the $S_0 \rightarrow {}^1L_a$ and $S_0 \rightarrow {}^1L_b$ states.[19] This example illustrates the additivity of anisotropies (eq. 10.6). This example is also impor-

tant for an understanding of the fluorescence from tryptophan residues in proteins (Chapter 16). At any excitation wavelength λ the observed anisotropy is

$$r_0(\lambda) = f_a(\lambda) r_{0a} + f_b(\lambda) r_{0b} \tag{10.23}$$

where $f_i(\lambda)$ represents the fractional contribution of the ith state to the total absorption at the wavelength λ, and r_{0i} represents the limiting anisotropy of this state. The assumption was made that r_{0a} and r_{0b} are independent of wavelength, that emission occurs only from the ^1L_a state, and that the quantum yield is independent of excitation wavelength. The highest observed value of r_0 was 0.3, and this value was assigned to r_{0a}. This means that absorption of the ^1L_a state is assumed to be dominant at excitation wavelengths of 300 nm and greater. Selection of a value for r_{0b} is more difficult since there is no obvious wavelength where the absorption of ^1L_b is dominant. The transition dipoles for ^1L_a and ^1L_b states are thought to be perpendicular. The anisotropy expected for ^1L_b can be predicted using eq. 10.22, which describes the loss in anisotropy due to an angular displacement of two oscillators by a known angle. The maximum value of r_0 (0.4) is replaced by r_{0a} = 0.3. Hence the anisotropy of the ^1L_b state is given by

$$r_{0b} = 0.30 \left(\frac{3\cos^2\beta - 1}{2} \right) \tag{10.24}$$

Using β = 90° one obtains r_{0b} = –0.15. These values of r_{0a} and r_{0b} are used in eq. 10.23, along with the restriction that the total fractional absorption is unity ($f_a(\lambda) + f_b(\lambda) = 1$), to calculate the fractional absorption of each state as a function of wavelength. Rearrangement of eq. 10.23 yields

$$f_a(\lambda) = \frac{r_0(\lambda) - r_{0b}}{r_{0a} - r_{0b}} = \frac{r_0(\lambda) + 0.15}{0.45} \tag{10.25}$$

$$f_b(\lambda) = \frac{r_{0a} - r_0(\lambda)}{r_{0a} - r_{0b}} = \frac{0.3 - r_0(\lambda)}{0.45} \tag{10.26}$$

And finally, the absorption spectrum of each state is given by

$$A_a(\lambda) = f_a(\lambda) A(\lambda) \tag{10.27}$$

$$A_b(\lambda) = f_b(\lambda) A(\lambda) \tag{10.28}$$

where $A(\lambda)$ is the total absorption spectrum. These resolved spectra are shown in the lower panel of Figure 10.10. The ^1L_b absorption is structured, but this absorption is less intense than the ^1L_a absorption. The peak at 290 nm in the absorption spectrum of indole is seen to be due to the ^1L_b state, and this peak absorption corresponds to a minimum in the r_0 value. Above 295 nm only the ^1L_a state absorbs, and the anisotropy is relatively constant. This is one reason why 295–300 nm excitation is used when studying the intrinsic tryptophan emission of proteins. This example illustrates how polarization spectra reveal the electronic properties of fluorophores.

10.4. MEASUREMENT OF FLUORESCENCE ANISOTROPIES

Prior to describing the applications of anisotropy, it is useful to understand the methods used to measure the anisotropy or polarization. We describe steady-state measurements, but similar considerations apply to time-resolved measurements of anisotropies. Two methods are commonly used. These are the L-format method, in which a single emission channel is used, and the T-format method, in which the parallel and perpendicular components are observed simultaneously through separate channels. The procedures described below are intended to correct for the different efficiencies of the instrumentation for detection of the various polarized components of the emission (Chapter 2).

10.4.1. L-Format or Single-Channel Method

The L format is used most frequently because most fluorometers have only a single emission channel. Assume the sample is excited with vertically polarized light, and the emission is observed through a monochromator (Figure 10.11). The monochromator will usually have a different transmission efficiency for vertically and horizontally polarized light. Consequently, rotation of the emission polarizer changes the measured intensities even if the sample emits unpolarized light. The measured intensities are not the desired parallel and perpendicular intensities, but rather intensities that are also proportional to the transmission efficiencies of the monochromator for each polarized component. The objective is to measure these actual intensities, $I_{\parallel}$ and $I_{\perp}$, unbiased by the detection system.

We use two subscripts to indicate the orientation of the excitation and emission polarizers, respectively. For exam-

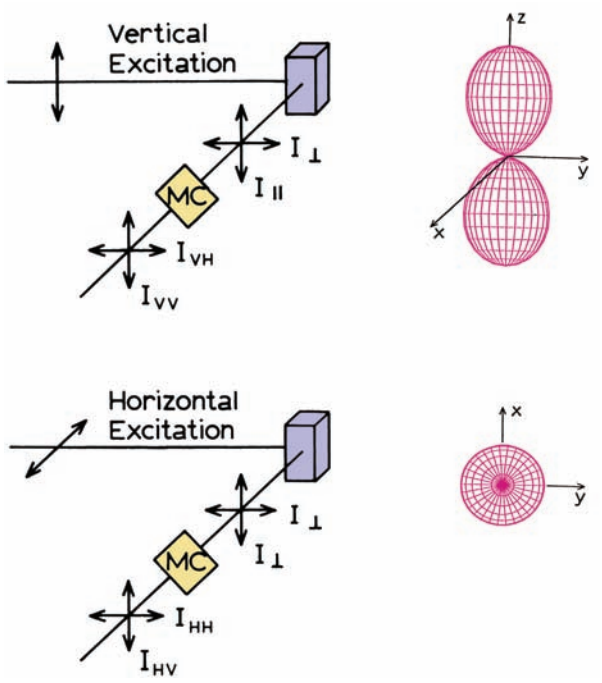

Figure 10.11. Schematic diagram for L-format measurements of fluorescence anisotropy. MC, monochromators. The shapes on the right are the excited-state distributions.

ple, I_{HV} corresponds to horizontally polarized excitation and vertically polarized emission. This notation is easy to recall since the order of the subscripts represents the order in which the light passes through the two polarizers. Let S_V and S_H be the sensitivities of the emission channel for the vertically and horizontally polarized components, respectively. For vertically polarized excitation the observed polarized intensities are

$$I_{VV} = kS_V I_{\parallel} \tag{10.29}$$

$$I_{VH} = kS_H I_{\perp} \tag{10.30}$$

where k is a proportionality factor to account for the quantum yield of the fluorophore and other instrumental factors aside from the polarization-dependent sensitivity. Division of 10.29 and 10.30 yields

$$\frac{I_{VV}}{I_{VH}} = \frac{S_V}{S_H}\frac{I_{\parallel}}{I_{\perp}} = G\frac{I_{\parallel}}{I_{\perp}} \tag{10.31}$$

The measured intensity ratio is different from the true value by a factor G. To calculate the actual intensity ratio ($I_{\parallel}/I_{\perp}$) we need to determine the G factor, which is the ratio of the sensitivities of the detection system for vertically and horizontally polarized light:

$$G = \frac{S_V}{S_H} \tag{10.32}$$

If the measured intensities are not corrected for the G factor, the calculated anisotropy will be incorrect. For instance, assume $G = 2.0$. This means that the emission monochromator passes vertically polarized light, at the chosen emission wavelength, with twofold greater efficiency than horizontally polarized light. The G factor is dependent upon the emission wavelength, and to some extent the bandpass of the monochromator. Frequently, anisotropy measurements are performed using an emission filter rather than a monochromator. Filters generally do not have a significant polarizing effect, and hence one expects $G = 1.0$. Nonetheless, this factor should always be determined since rotation of the emission polarizer can cause the focused image of the fluorescence to change position, altering the effective sensitivity.

The G factor is easily measured using horizontally polarized excitation. With horizontally polarized excitation the excited-state distribution is rotated to lie along the observation axis. When this is done both the horizontally and vertically polarized components are equal and proportional to $I_{\perp}$ (Figure 10.11). These components are equal because the electric field is equally distributed around the observation axis. Both polarizer orientations are perpendicular to the polarization of the excitation. Any measured difference in I_{HV} and I_{HH} must be due to the detection system. Specifically,

$$\frac{I_{HV}}{I_{HH}} = \frac{S_V}{S_H}\frac{I_{\perp}}{I_{\perp}} = \frac{S_V}{S_H} = G \tag{10.33}$$

Frequently the excitation intensity can change when the excitation polarizer is rotated. This change is a constant factor in the numerator and denominator of eq. 10.33, and hence cancels. When the G factor is known the ratio $I_{\parallel}/I_{\perp}$ can be calculated using

$$\frac{I_{VV}}{I_{VH}}\frac{1}{G} = \frac{I_{VV}I_{HH}}{I_{VH}I_{HV}} = I_{\parallel}/I_{\perp} \tag{10.34}$$

The anisotropy is given by

$$r = \frac{I_{\parallel}/I_{\perp} - 1}{I_{\parallel}/I_{\perp} + 2} \tag{10.35}$$

which is frequently used in the alternative form:

$$r = \frac{I_{VV} - GI_{VH}}{I_{VV} + 2GI_{VH}} \tag{10.36}$$

10.4.2. T-Format or Two-Channel Anisotropies

In the T-format method the intensities of the parallel and perpendicular components are measured simultaneously using two separate detection systems (Figure 10.12). The emission polarizers are left unchanged, so the sensitivity of each channel remains the same during the measurement. It is still necessary to measure the relative sensitivity of the two detection systems, which is accomplished using horizontally polarized excitation. The T-format measurements are performed as follows. The excitation polarizer is first placed in the vertical orientation to measure the ratio of the parallel and perpendicular signals (R_V). This ratio is given by

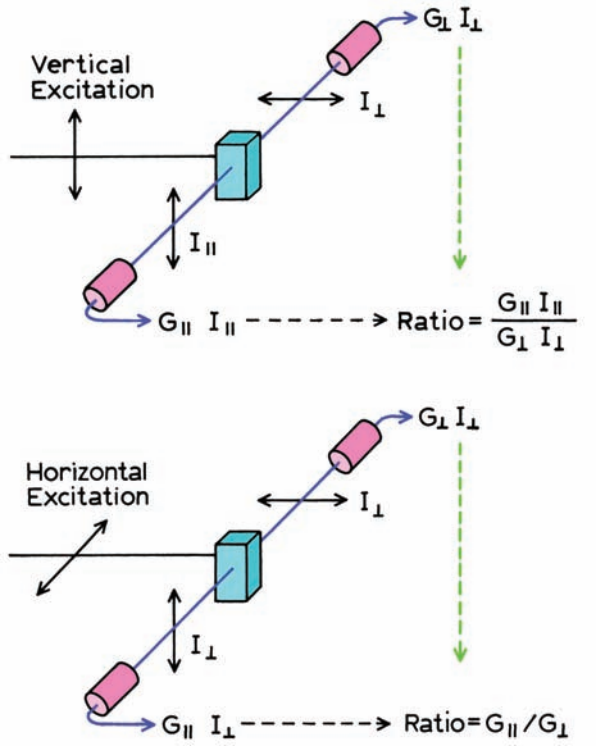

Figure 10.12. Schematic diagram for T-format measurements of fluorescence anisotropy.

$$R_V = \frac{G_{\parallel} I_{\parallel}}{G_{\perp} I_{\perp}} \tag{10.37}$$

where $G_{\parallel}$ and $G_{\perp}$ are the sensitivities of the parallel and perpendicular channels, respectively. This ratio can be adjusted to unity, but in practice it is easier to simply measure the ratio. This ratio is measured again using horizontally polarized excitation. Then both emission channels observe $I_{\perp}$ (Figure 10.12). Hence the ratio of intensities is given by

$$R_H = G_{\parallel}/G_{\perp} \tag{10.38}$$

Division of 10.37 by 10.38 yields

$$\frac{R_V}{R_H} = \frac{I_{\parallel}}{I_{\perp}} \tag{10.39}$$

which can be used to calculate the anisotropy (eq. 10.35). The excitation intensity may vary upon rotation of the excitation polarizer. This factor cancels in taking the ratio. However, difficulties can arise if light from the excitation monochromator is completely polarized in either the vertical or horizontal direction (Chapter 2). Then either R_H or R_V cannot be measured because of inadequate light intensity. This difficulty can be avoided by using a different excitation wavelength where adequate intensity is available for each polarization. This is acceptable because R_V and R_H are properties of the detection system, and are not dependent on the excitation wavelength or the degree of polarization displayed by the sample. The theoretical maximum for $I_{\parallel}/I_{\perp}$ is 3 ($r = 0.4$). Values of $I_{\parallel}/I_{\perp}$ in excess of 3 generally indicate an artifact, typically scattered light. Scattered light is 100% polarized ($I_{\parallel}/I_{\perp} = \infty$, $r = 1.0$), and a small percentage of such light can seriously distort the anisotropy values.

10.4.3. Comparison of T-Format and L-Format Measurements

For fluorometers with a single emission channel the L format must be used to measure anisotropies. This procedure requires four individual measurements: I_{VV}, I_{VH}, I_{HV}, and I_{HH}. The latter two determine the G factor, which does not need to be measured each time. The T-format method again requires four intensity measurements, which appear as two

ratios. Because of the simultaneous measurement, fluctuations in signal intensity are canceled in T-format measurements. In the early days of fluorescence spectroscopy T-format measurements were preferred. With modern instruments there no longer seems to be any significant advantage to T-format measurements, except possibly for a decreased time for data acquisition. L-format measurements are routinely used in this laboratory.

10.4.4. Alignment of Polarizers

Accurate measurement of fluorescence anisotropies requires that the polarizers be precisely positioned in the vertical and horizontal orientations. The alignment can be easily checked and adjusted using a dilute suspension of glycogen or colloidal silica in water. The scattered light is 100% polarized, that is, $r = 1.0$. In this laboratory we consider the alignment to be adequate when the measured value is 0.97 or larger. It is essential to use dilute suspensions of scatterer. Otherwise multiple scattering events lead to decreased values of polarization.

Alignment can be accomplished as follows. The excitation polarizer is rotated to the approximate vertical position. Precise vertical alignment is not necessary since the scattered light is vertically polarized. The angular alignment of the emission polarizer is adjusted so that the minimum intensity is observed. This is the horizontal position. It is preferable to use this minimum intensity for alignment. The maximum intensity for the vertical component is less sharply defined. One should check that the vertical polarizer stop is also properly adjusted. Rotation of the emission polarizer should now yield the maximum and minimum intensities when the polarizer is at the vertical and horizontal stops, respectively. These adjustments should be performed with the emission monochromator removed, or its wavelength chosen for approximate equal transmission efficiencies for vertically and horizontally polarized light. Otherwise, the polarizing properties of the emission monochromator could interfere with the alignment. The wavelength selection for equal transmission efficiencies can be accomplished using either horizontally polarized excitation, to obtain $I_{\parallel} = I_{\perp}$, or a sample whose emission is not polarized. Examples of such solutions are 9-cyanoanthracene in the fluid solvent ethanol or $[Ru(bpy)_3]^{2+}$ in water.[11]

Alignment of the excitation polarizer is performed in a similar manner. The emission polarizer should be set in the vertical position. The minimum and maximum intensities of scattered light should be observed when the excitation polarizer is at its horizontal and vertical stops, respectively. Once again one should consider the polarization properties of the excitation monochromator.

10.4.5. Magic-Angle Polarizer Conditions

The goal of intensity measurements is usually to measure a signal proportional to the total intensity (I_T), and not proportional to $I_{\parallel}$ or $I_{\perp}$. However, since the transmission efficiency of the emission monochromator depends on polarization, the observed signal is not exactly proportional to $I_{\parallel} + 2I_{\perp}$, but rather to some other combination of $I_{\parallel}$ and $I_{\perp}$. By the use of polarizers the measured intensity can be proportional to the total intensity, $I_T = I_{\parallel} + 2I_{\perp}$, irrespective of the degree of polarization of the sample. To accomplish this the excitation polarizer is oriented in the vertical position and the emission polarizer is oriented (54.7°) from the vertical. Since $\cos^2 54.7° = 0.333$ and $\sin^2 54.7° = 0.667$, these polarizer settings result in $I_{\perp}$ being selected twofold over $I_{\parallel}$, forming the correct sum for $I_T = I_{\parallel} + 2I_{\perp}$. The use of magic-angle conditions is especially important for intensity decay measurements. The intensity decays of the vertically and horizontally polarized components are usually distinct. If $I_{\parallel}(t)$ and $I_{\perp}(t)$ are not properly weighted, then incorrect decay times are recovered. If the anisotropy is zero, then the correct intensity and intensity decay times are recovered independent of polarizer orientation.

10.4.6. Why is the Total Intensity Equal to $I_{\parallel} + 2I_{\perp}$?

It is widely known that the total intensity is given by $I_{\parallel} + 2I_{\perp}$, but the origin of this result is less widely understood. It is actually quite simple. For any fluorophore the total intensity is equal to the sum of the intensities along the three axes: $I_T = I_x + I_y + I_z$. Each intensity is given by the square of the transition moment projection on each axis. Using these terms from Figure 10.4, the sum of the three projections is unity. This is true for every fluorophore, so that if the three intensities are measured all fluorophores contribute equally to the total intensity, regardless of this orientation. Now suppose the sample has z-axis symmetry. Then $I_z = I_{\parallel} + 2I_{\perp}$.

10.4.7. Effect of Resonance Energy Transfer on the Anisotropy

In Section 10.3 we discussed an intrinsic cause of depolarization, namely, angular displacement between the absorp-

tion and emission moments. The fluorophores were assumed to be immobile and the excited state was assumed to remain localized on the originally excited fluorophore. The anisotropy can also be decreased by extrinsic factors that act during the lifetime of the excited state. These include rotational diffusion of the fluorophore and the resonance energy transfer (RET) of energy among fluorophores (Chapter 13). Both processes result in additional angular displacement of the emission oscillator and hence lower anisotropies.

The effects of rotational diffusion and energy transfer are easily separated by selection of the experimental conditions. For example, Brownian rotations cause negligible depolarization when the rotational rate is much slower than the rate of fluorescence emission. Therefore, rotation diffusion can be decreased or eliminated using low temperatures and/or high viscosities. Radiationless energy transfer occurs only in concentrated solution where the average distance between the fluorophore molecules is comparable to a characteristic distance R_0, which is typically near 40 Å. Millimolar fluorophore concentrations are required to obtain this average distance (Chapter 13). This concentration is considerably larger than the usual concentrations required for fluorescence measurements, which are about 10^{-6} M. Hence radiationless energy transfer is easily avoided by the use of dilute solutions. The solutions also need to be adequately diluted so that radiative transfer does not occur.

The effect of RET on the anisotropy is illustrated by the excitation anisotropy spectrum of fluorescein in dilute and concentrated solution.[25] Fluorescein is subject to radiative (emission and reabsorption) and non-radiative energy transfer because of the small Stokes shift. In this experiment (Figure 10.13) radiative transfer was avoided by using thin samples, and rotational diffusion was eliminated by using a vitrified sample. Under these experimental conditions RET is the only mechanism that can decrease the anisotropy. In dilute solution fluorescein displays its characteristic anisotropy spectrum, with high anisotropy for excitation above 380 nm. At high concentration the anisotropy is decreased. This effect is due to RET between fluorescein molecules. In random solution it is known that a single non-radiative transfer step reduces the anisotropy to 4% of the initial value.[26–29] Hence RET is an effective mechanism in depolarization. The presence or absence of RET can usually be predicted from the concentration in the sample and the spectral properties of the probes.

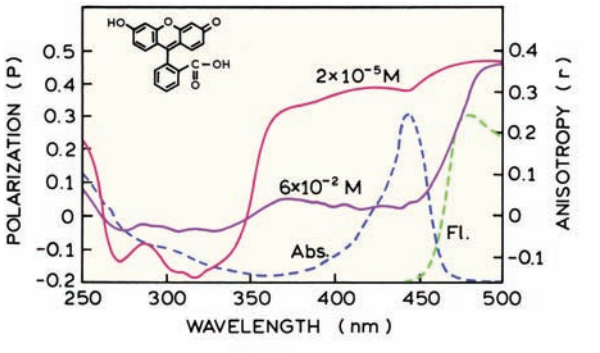

Figure 10.13. Excitation polarization spectra of fluorescein in propylene glycol at –50°C. Radiative transfer was avoided by using thin samples, 30 to 50 microns thick. Revised and reprinted with permission from [25].

Examination of Figure 10.13 reveals that the anisotropy (polarization) of the concentrated sample increases for excitation wavelengths longer than 460 nm. This increase is due to the failure of energy transfer with red edge excitation (Chapter 7). The anisotropy increases because the red-edge excitation results in a shift of the emission spectrum to longer wavelength, decreased spectral overlap, and less energy transfer.

10.4.8. Trivial Causes of Depolarization

The measured anisotropies can be lower than the actual values for several trivial reasons, including light scattering, reabsorption, and misalignment of the polarizers. While these are nontrivial experimental problems, they are dependent only on the optical conditions of the experiment and do not provide useful information on the molecular properties of the sample.

Biological samples, such as aqueous suspensions of membranes, are frequently turbid. This turbidity can cause scattering of both the incident light and the emitted photons. The scattered incident light can result in excitation, and the emitted photons can be scattered prior to observation. Each scattering event is thought to decrease the anisotropy of the scattered photon from 0.85 to 0.7 of the value in the absence of scatter.[30–31] The magnitude of the effect depends on the size of the scatterer. The observed anisotropy is expected to decrease linearly with the optical density due to turbidity. The actual proportionality constant will depend upon the sample under investigation.[32] It is therefore advisable to investigate the effect of turbidity for

any sample which displays visible turbidity. This can be accomplished by either actual dilution of the sample or using a cuvette with smaller dimensions. If dilution does not change in anisotropy, then there is unlikely to be significant depolarization due to scattering.

A more serious effect of scattering is the possibility that scattered light reaches the detector. This is particularly true for dilute solutions where the intensity is low, and scattering from the optics and sample can be significant. Since the scattered light will be highly polarized ($r = 1.0$), a small percentage of scattered light can result in significant changes in the anisotropy (eq. 10.6, see also Problem 10.2). If scattered light reaches the detector, then the measured anisotropy will usually increase relative to its true value.

Another trivial cause of depolarization is radiative transfer, which is the reabsorption of emitted photons. It is more difficult to eliminate radiative transfer since it can occur at lower concentrations than RET. In fact, radiative transfer is a frequent cause of low anisotropy values for fluorescein. Because of their large spectral overlap, fluorescein solutions often show the effects of radiative transfer. Surprisingly, radiative transfer is less effective than RET in depolarization. A single radiative transfer step reduces the anisotropy to 28% of its initial value,[33–34] as compared to 4% of the initial value for a single RET step.

Measured anisotropy values can also be too low due to misalignment or inefficiency of the polarizers. Film polarizers become less ideal at short wavelengths. The polarizers can be tested by examination of a dilute scattering solution (Section 10.4.4.). And, finally, one should always examine a blank sample that scatters light approximately the same as the sample. Background signals can be especially problematic for anisotropy measurements. The background signal may be polarized if due to scattered light, or unpolarized if due to low-molecular-weight impurities. Hence, background signals can either increase or decrease the anisotropy. In order to correct for background it is necessary to measure the four individual intensities from the blank sample, and subtract them from each respective intensity value in eq. 10.36.

10.4.9. Factors Affecting the Anisotropy

The various factors that can affect the anisotropy were summarized in an insightful table,[3] which outlines the experimental conditions for various anisotropy measurements (Table 10.2). The fundamental anisotropy can be measured in dilute highly viscous solution, where rotational diffusion or RET do not occur. Information about the Förster distance (R_0) for hetero- or homo-RET can be obtained from studies in concentrated viscous solution. The most interesting condition designated in Table 10.2 is that for dilute non-viscous solutions. In such solutions the anisotropy is primarily determined by rotational motion of the fluorophore. For labeled proteins these motions are dependent upon the size and shape of the protein, its extent of aggregation, and other factors. For membranes the anisotropy depends upon the chemical composition and phase state of the membranes. As a result, anisotropy measurements are frequently used to study the properties and interactions of biological macromolecules.

10.5. EFFECTS OF ROTATIONAL DIFFUSION ON FLUORESCENCE ANISOTROPIES: THE PERRIN EQUATION

Rotational diffusion of fluorophores is a dominant cause of fluorescence depolarization, and most applications depend

Table 10.2. Extrinsic Causes of Depolarization[a]

Condition	Observable	Molecular property
Dilute viscous solution (propylene glycol, –70° C)	r_0 or cos β (eq. 10.22)	Angle between absorption and emission dipole as a function of excitation wavelength
Concentrated viscous solution	$0 < \|r\| < \|r_0\|$ Anisotropy decreased by energy migration	Distance dependence of radiationless energy transfer
Dilute non-viscous solution (H_2O, EtOH, room temp.)	$0 < \|r\| < \|r_0\|$ Anisotropy decreased due to Brownian rotation	Size and shape of fluorophore or macromolecule

[a]From [3].

on changes in the rate of rotation. Depolarization by rotational diffusion of spherical rotors is described by the Perrin equation:[35–37]

$$\frac{r_0}{r} = 1 + \tau/\theta = 1 + 6D\tau \tag{10.40}$$

where τ is the fluorescence lifetime, θ is the rotational correlation time, and D is the rotational diffusion coefficient. If the correlation time is much larger than the lifetime ($\theta >> \tau$), then the measured anisotropy (r) is equal to the fundamental anisotropy (r_0). If the correlation time is much shorter than the lifetime ($\theta << \tau$), then the anisotropy is zero.

The Perrin equation can be derived from first principles based on diffusional steps.[3,38] A simple derivation is possible using the time-resolved decay of anisotropy $r(t)$ for a spherical molecule:

$$r(t) = r_0 e^{-t/\theta} = r_0 e^{-6Dt} \tag{10.41}$$

In this equation the rotational correlation time of the fluorophore (θ) is given by

$$\theta = \frac{\eta V}{RT} \tag{10.42}$$

where η is the viscosity, T is the temperature in °K, R is the gas constant, and V is the volume of the rotating unit. The rotational correlation time is related to the rotational diffusion coefficient by $\theta = (6D)^{-1}$. Only spherical molecules display a single exponential anisotropy decay. More complex expressions are predicted for nonsymmetric species or molecules (Chapter 12).

The steady-state anisotropy can be calculated from an average of the anisotropy decay, $r(t)$, over the intensity decay, $I(t)$:

$$r = \frac{\int_0^\infty I(t) r(t)\, dt}{\int_0^\infty I(t)\, dt} \tag{10.43}$$

For a single-exponential intensity decay, substitution into eq. 10.43 yields

$$r = \frac{r_0}{1 + \tau/\theta} \tag{10.44}$$

which is a form of the Perrin equation. Using this equation, it is possible to calculate the anisotropy expected for fluorophores in solvents or for labeled macromolecules, assuming the molecules are spherical. For example, perylene has a lifetime of 6 ns and $r_0 = 0.36$. In ethanol rotational diffusion is expected to decrease the anisotropy to 0.005 (Problem 10.5).

10.5.1. The Perrin Equation: Rotational Motions of Proteins

Prior to the availability of time-resolved measurements the apparent molecular volumes of proteins were measured using the Perrin equation. This application can be seen by rearranging eq. 10.44:

$$\frac{1}{r} = \frac{1}{r_0} + \frac{\tau}{r_0\theta} \tag{10.45}$$

For globular proteins the rotational correlation time is approximately related to the molecular weight (M) of the protein by

$$\theta = \frac{\eta V}{RT} = \frac{\eta M}{RT}(\bar{v} + h) \tag{10.46}$$

where $\bar{v}$ is the specific volume of the protein, and h is the hydration, T is the temperature in °K, $R = 8.31 \times 10^7$ erg/mol°K, and the viscosity η is in poise (P). Values of h for proteins are typically near 0.73 ml/g, and the hydration is near 0.23 g H_2O per gram of protein. This expression predicts that the correlation time of a hydrated protein is about 30% larger than that expected for an anhydrous sphere. Generally, the observed values of θ are about twice that expected for an anhydrous sphere.[39] For example, for an anhydrous protein sphere with a 50 kD molecular weight, with $h = 0.73$ ml/g and $\eta = 0.94$ cP, the calculated rotational correlation time at 25°C is near 14 ns. The anisotropy decay of an immunoglobulin F_{ab} fragment, labeled at the antigen binding site with dansyl-lysine, yielded a rotational correlation time of 33 ns. This larger correlation time was consistent with a hydration of 0.32 ml/g and an axial ratio near 2. This result is typical of that found for proteins (Table 10.3), and is probably a result of the non-spherical shape of most proteins and a larger effective solvent shell for rotational diffusion than for hydration. For convenience we have listed the calculated rotation correlation times for proteins with different molecular weights and different amounts of hydration in Table 10.4.

Table 10.3. Rotational Correlation Times for Proteins[a]

Protein	Molecular weight	Observed θ (ns)	$\theta_{obs}/\theta_{calc}$
Apomyoglobin	17,000	8.3	1.9
β-Lactoglobulin (monomer)	18,400	8.5	1.8
Trypsin	25,000	12.9	2.0
Chymotrypsin	25,000	15.1	2.3
Carbonic anhydrase	30,000	11.2	1.4
β-Lactoglobulin (dimer)	36,000	20.3	2.1
Apoperoxidase	40,000	25.2	2.4
Serum albumin	66,000	41.7	2.4

[a]θ_{obs} is the observed rotational correlation time, adjusted to T/η corresponding to water at 25°C. θ_{calc} is the rotational correlation time calculated for a rigid unhydrated sphere with a molecular weight of the protein, assuming a partial specific volume of 0.73 ml/g. From [39].

Table 10.4. Calculated Rotational Correlation Times for Proteins[a]

T	Molecular weight (kD)	Correlation time θ (ns) $h = 0$	$h = 0.2$	$h = 0.4$
2°C	10	5.5	6.9	8.4
	25	13.7	17.3	21.1
	50	27.4	34.6	42.0
	100	54.8	69.2	84.0
	500	274.0	346.0	420.0
20°C	10	3.1	3.9	4.7
	25	7.0	9.7	11.8
	50	15.4	19.5	23.6
	100	30.8	39.0	47.2
	500	154.0	195.0	236.0
37°C	10	2.0	2.5	3.1
	25	5.0	6.4	7.7
	50	10.0	12.7	15.4
	100	20.1	25.4	30.8
	500	100.5	127.0	154.0

[a]Calculated using $\theta = \eta M(\bar{v} + h)/RT$ with $\bar{v} = 0.75$ ml/g, and various degrees of hydration (h). The viscosities are η (2°C) = 1.67 cP, η (20°C) = 1.00 cP, η (37°C) = 0.69 cP.

The apparent volume of a protein can be determined by measuring the anisotropy at various temperatures and/or viscosities. Substitution of eq. 10.42 into 10.45 yields a modified form of the Perrin equation:

$$\frac{1}{r} = \frac{1}{r_0} + \frac{\tau RT}{r_0 \eta V} \tag{10.47}$$

The use of eq. 10.47 was one of the earliest biochemical applications of fluorescence.[40–42] The general approach is to covalently label the protein with an extrinsic fluorophore. The fluorophore is chosen primarily on the basis of its fluorescence lifetime. This lifetime should be comparable to the expected rotational correlation time of the protein. In this way the anisotropy will be sensitive to changes in the correlation time. Generally, the fluorescence anisotropies are measured over a range of T/η values. Temperature is varied in the usual manner, and viscosity is generally varied by addition of sucrose or glycerol. For biochemical samples only a limited range of T/τ values are available. At high temperature the macromolecule may denature, and at low temperatures the solvent may freeze or the macromolecule may not be soluble. The apparent volume of the protein is obtained from a plot of $1/r$ versus T/η (Figure 10.14). The intercept of the y-axis represents extrapolation to a very high viscosity, and should thus be $1/r_0$, where r_0 is the fundamental anisotropy of the fluorophore. In practice fluorophores bound to protein often display segmental motions, which are independent of overall rotational diffusion. These motions are often much faster than rotational diffusion, and rather insensitive to the macroscopic viscosity. As shown in Chapter 12, such motions can be considered to be an independent factor which depolarizes the emission by a constant factor. The effect is to shift $1/r$ to larger values, and shift the apparent r_0 value to a smaller value (larger y-intercept). This does not mean that the r_0 value is in fact smaller, but rather reflects the inability of the Perrin plot to resolve the faster motion.

What value of r_0 should be used to calculate the volume of the protein? In general the extrapolated value of r_0 (r_0^{app}) will yield the best estimate of the volume because this value accounts for segmental motion of the probe and partially cancels the effects of this motion on the correlation time θ.

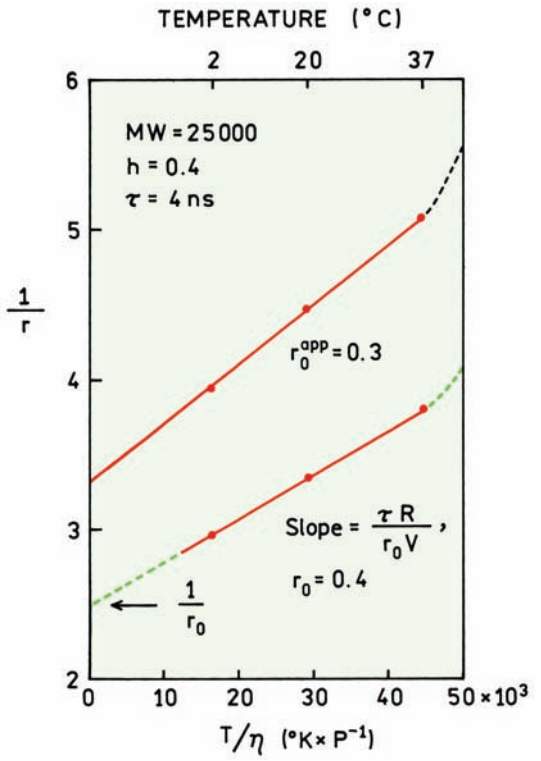

Figure 10.14. Perrin plots for determination of protein volume. The curves are drawn for a protein molecular weight of 25,000 daltons in water, $h = 0.4$ and $\tau = 4$ ns. The value of $r_0 = 0.4$ represents a rigidly bound probe and $r_0 = 0.3$ represents a probe with some segmented mobility. The upward curving dashed lines indicate the protein is denaturing at high temperature.

For example, assume the segmental motion of the fluorophore is much more rapid than the rotational diffusion of the protein. Then, the value of r_0 is effectively reduced to

$$r_0^{app} = r_0\left(\frac{<3\cos^2\alpha> - 1}{2}\right) \qquad (10.48)$$

where α is the angle through which the probe undergoes this segmental motion. The term $(1/r_0^{app})$ cancels in the calculation of the molecular volume, and the apparent volume represents overall rotation diffusion of the protein. It is important to note that, if the short correlation time for segmental motion (θ_S) is not much faster than the overall correlation time (θ_L), then the apparent volume can be substantially decreased due to contributions from the more rapid motions (Section 10.9). Some information is available by comparison of the extrapolated and frozen solution values of r_0. If r_0^{app} is much smaller than r_0 one may infer the existence of segmental motions of the probe on the macromolecule, independent motions of domains of the protein, or possibly RET in multiply labeled proteins. Another behavior seen in Perrin plots is a rapid increase in $1/r$ at high temperatures. Such an increase is usually the result of denaturation of the macromolecule, resulting in an increase in independent motion of the probe and a decrease in the anisotropy.

A different version of the Perrin equation is often found in the older literature:

$$\left(\frac{1}{P} - \frac{1}{3}\right) = \left(\frac{1}{P_0} - \frac{1}{3}\right)\left(1 + \frac{\tau RT}{\eta V}\right)$$

$$= \left(\frac{1}{P_0} - \frac{1}{3}\right)\left(1 + \frac{3\tau}{\rho}\right) \qquad (10.49)$$

This equation is equivalent to eq. 10.47, except for the use of polarization in place of anisotropy. When using the equation, a plot $(1/P - 1/3)$ versus T/η is used to obtain the molecular volume. The intercept yields the apparent value of $(1/P_0^{app} - 1/3)$, which can be larger than the true value $(1/P_0 - 1/3)$ if there is segmental motion of the probe. The term ρ is the rotational relaxation time ($\rho = 3\theta$). At present the use of anisotropy, the rotational correlation time, and eq. 10.44 is preferred.

10.5.2. Examples of a Perrin Plot

It is instructive to examine a representative Perrin plot (Figure 10.15).[16] These data are for 9-anthroyloxy stearic acid in a viscous paraffin oil, Primol 342. The anisotropies were measured at various excitation wavelengths, corresponding to different r_0 values (Figure 10.8). The y-axis intercepts are different because of the different r_0 values. Also, the slopes are larger for shorter excitation wavelengths because the value of r_0 appears in the denominator of eq. 10.47. In spite of the very different values of $1/r$ for different excitation wavelengths, the data are all consistent with a correlation time near 15 ns at 25 °C (Table 10.5). For a spherical molecule, the correlation time is independent of r_0. In Chapter 12 we will see that the correlation times can depend on the value of r_0 for non-spherical molecules. This effect may be the cause of the somewhat different correlation times found for different excitation wavelengths.

The y-axis intercepts yield the apparent values of r_0 extrapolated to high viscosity, which can be compared with measured values in a glassy solvent (Table 10.5). The

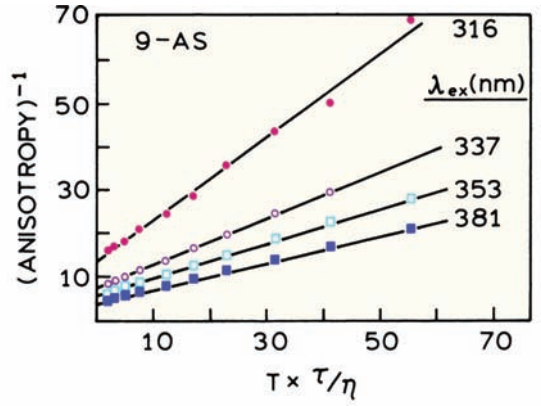

Figure 10.15. Perrin plots of 9-anthroyloxy stearic acid in Primol 342. The excitation wavelengths were 316 (●), 337 (○), 353 (□) and 381 nm (■). The lifetime, ranging from 10.5 to 9.7 ns, is incorporated into the *x*-axis. Revised and reprinted with permission from [16]. Copyright © 1982, American Chemical Society.

Table 10.5. Fundamental (r_0) and Extrapolated (r_0^{app}) Anisotropy Values and Rotational Correlation Times for Anthroyloxy Stearic Acid[a]

Excitation wavelength (nm)	r_0	r_0^{app}	θ (ns)[b]
316	0.090	0.075	13
337	0.178	0.136	14
353	0.231	0.179	14
381	0.323	0.242	18

[a]From [16].
[b]In Primol 342 at 6°C.

extrapolated values are about 25% lower than the measured r_0 values. This is a typical result for Perrin plots. Fluorophores are often non-spherical, resulting in multi-exponential anisotropy decays. In such cases the Perrin plots are curved toward the *x*-axis, resulting in higher apparent intercepts on the *y*-axis.

10.6. PERRIN PLOTS OF PROTEINS

10.6.1. Binding of tRNA to tRNA Synthetase

Perrin plots of labeled macromolecules have been extensively used to determine the apparent hydrodynamic volumes. One example is the binding of methionine tRNA ($tRNA^{fMet}$) with methionyl-tRNA synthetase (met-RS). The 3' end of the tRNA was labeled with fluorescein (Fl) by periodate oxidation of the tRNA followed by reaction with

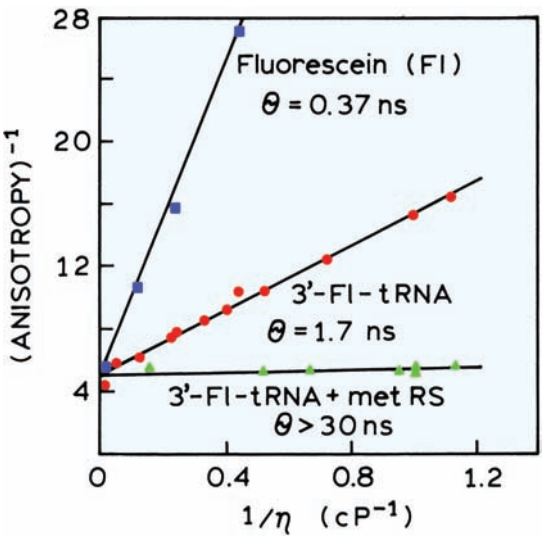

Figure 10.16. Perrin plot of fluorescein (Fl, ■) and $tRNA^{fMet}$ labeled at the 3' end with fluorescein (●). Also shown is the labeled t-RNA when bound to methionyl-tRNA synthetase (met RS, ▲). The experiments were performed at 20°C. The viscosity η was varied by adding sucrose. Excitation at 480 nm and emission at 520 nm. Revised and reprinted with permission from [43]. Copyright © 1986, American Chemical Society.

fluorescein thiosemicarbazide.[43] The Perrin plots were obtained at a single temperature with the viscosity changed by adding sucrose. As expected, fluorescein free in solution displays a subnanosecond correlation time (Figure 10.16). More surprising is the apparent correlation time for 3'-Fl-tRNA, which is 1.7 ns. Based on the size and shape of tRNA, the rotational correlation time is expected to be near 25 ns. This result indicates that the 3'-fluorescein label displays significant segmental freedom independent of overall rotational diffusion of the tRNA and that these segmental motions are the dominant cause for depolarization.

Upon binding of 3'-Fl-tRNA to the synthetase the anisotropy increases dramatically from 0.062 to 0.197. The small slope of the Perrin plot indicates that the correlation time is larger than 30 ns. The synthetase consists of two identical subunits, 76 kD each, so that its rotational correlation time is expected to be 100 ns or longer. Apparently, the 3' end of the tRNA interacts with the synthetase, immobilizing the fluorescein residue. It should be noted that the lifetime of fluorescein, typically near 3 ns, is too short to accurately measure the rotational correlation time of the complex. Based on eq. 10.44 the anisotropy of a 3-ns fluorophore will be decreased by only 3% for a correlation time of 100 ns. For this reason the correlation time is only stated as over 30 ns in Figure 10.16.

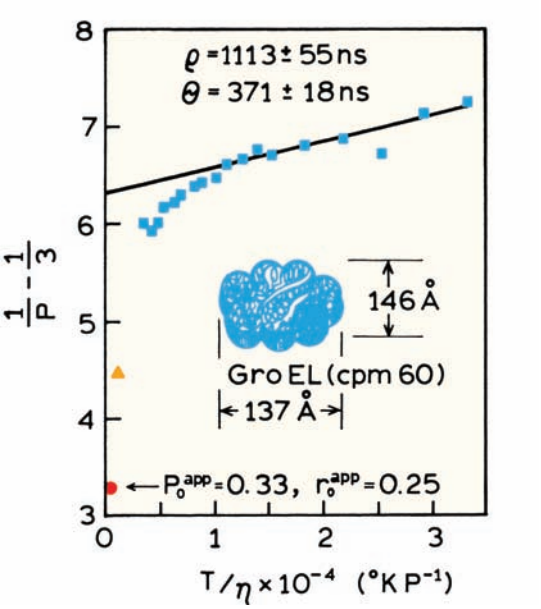

Figure 10.17. Perrin plot of chaperonin cpn60 labeled with 1-pyrenesulfonyl chloride at 25°C. Viscosities were varied with sucrose. Two points (● and ▼) were measured at 0°C. The pyrene lifetime was near 45 ns. Revised from [47].

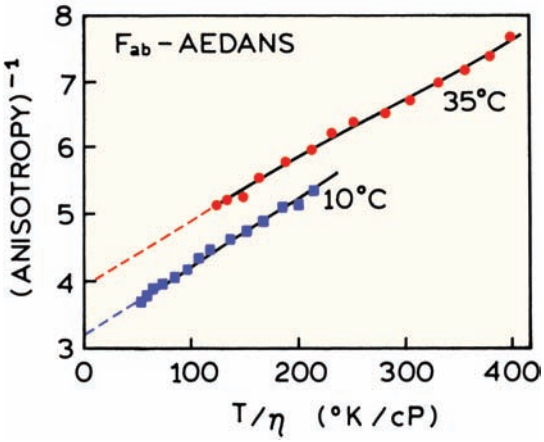

Figure 10.18. Perrin plots of immunoglobulin F_{ab} fragments labeled with AEDANS at the C terminus. Viscosity was varied by adding sucrose. Revised and reprinted with permission from [48]. Copyright © 1995, American Chemical Society.

The *y*-intercepts of the Perrin plots yield the apparent r_0 values, which are near 0.2 for these three fluorescein samples. This value is less than that typical of fluorescein, which is near 0.35. Hence, there appears to be some unresolved motion of the fluorescein even when bound to the synthetase. It is difficult to determine the *y*-intercept for fluorescein itself due to the large extent of depolarization.

10.6.2. Molecular Chaperonin cpn60 (GroEL)

Molecular chaperonins are proteins that assist other proteins in folding.[44–45] The cpn60 chaperonin (GroEL) from *E. coli* is a large multi-subunit oligomer consisting of fourteen identical 60-kD subunits. These subunits are arranged in two stacked rings, each with seven subunits. Each subunit consists of three domains. The entire protein of 840 kD is a cylindrical oligomer, 146 Å tall, 137 Å wide, with a central channel 45 Å in diameter.[46]

Rotational diffusion of cpn60 was studied using a pyrene-labeled protein.[47] Pyrene was chosen for its long fluorescence lifetime, which can reach 200 ns. In this case the pyrenesulfonyl label displayed a lifetime near 45 ns. The Perrin plot for pyrene-labeled cpn60 shows significant curvature (Figure 10.17). In this figure the data are presented in the older style using polarization instead of anisotropy. The chaperonin displays considerable flexibility, as can be seen from the curvature in the Perrin plot. Different apparent correlation times can be obtained for different regions of the curve. At lower viscosities the faster motions are complete, so that the overall rotational correlation time can be estimated from the limiting slope. This calculation results in an apparent correlation time near 370 ns. Calculation of the correlation time using eq. 10.46, with 0.23 g H_2O/g protein hydration, yields a correlation time near 347 ns. Hence, the slope from the Perrin plot observed for the lower viscosities provided a reasonable estimate of the overall size. The data at higher viscosity or lower temperature indicate the domain or subunits of cpn60 have significant independent mobility.

10.6.3. Perrin Plots of an F_{ab} Immunoglobulin Fragment

A potentially confusing aspect of the Perrin plots is the use of T/η as the *x*-axis. This implies that the same result should be obtained independent of whether temperature or viscosity is varied. Unfortunately, this is not usually the case. In fact, it is common to observe different Perrin plots for variation in temperature as compared to variation in viscosity. This is illustrated by the Perrin plots of F_{ab} fragments labeled with IAEDANS. These F_{ab} fragments show segmental motions that depend on temperature.[48] F_{ab} fragments are the antibody-binding domains of immunoglobulins. Different Perrin plots are observed at 10 and 35°C (Figure 10.18). At the higher temperature there is more independent motion

of the probe and/or domains of the F_{ab} fragment. Hence, the *y*-intercepts are larger. Perrin plots that depend differently on temperature or viscosity should not be regarded as incorrect, but rather as reflecting the temperature-dependent dynamics of the protein.

10.7. BIOCHEMICAL APPLICATIONS OF STEADY-STATE ANISOTROPIES

Anisotropy measurements are ideally suited for measuring the association of proteins with other macromolecules. This is because the anisotropy almost always changes in response to a change in correlation time. Also, the experiments are simplified by the independence of the anisotropy from the overall protein concentration.

10.7.1. Peptide Binding to Calmodulin

The use of anisotropy to study protein binding is illustrated by calmodulin. This protein activates a number of intracellular enzymes in response to calcium. One example is myosin light-chain kinase (MLCK).[49] The amino-acid (RS20) sequence that binds to calmodulin contains a single tryptophan residue (Figure 10.19). Since calmodulin contains only tyrosine, the peptide (RS20) can be selectively observed by excitation at 295 nm (Chapter 16). Upon addition of calmodulin the emission intensity at RS20 increases and the emission shifts to shorter wavelengths. These changes indicate a shielded environment for the tryptophan

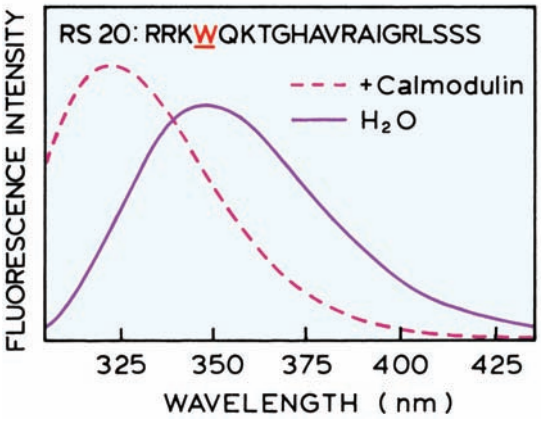

Figure 10.19. Emission spectra of the myosin light-chain kinase (MLCK) peptide RS20 in solution (solid) and bound to calmodulin in the presence of calcium (dashed). Excitation at 295 nm. Revised and reprinted with permission from [49]. Copyright © 1986, American Chemical Society.

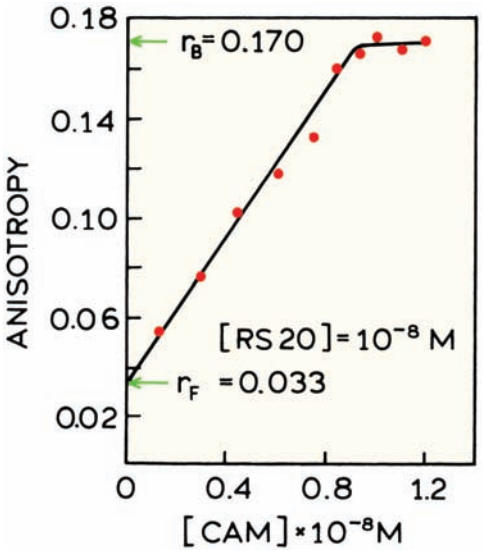

Figure 10.20. Titration of the MLCK peptide RS20 with calmodulin. Revised and reprinted with permission from [49]. Copyright © 1986, American Chemical Society.

residue in the complex. The anisotropy of RS20 increases dramatically on addition of calmodulin (Figure 10.20). These data can be used to determine that the stoichiometry of binding is 1:1. The sharp nature of the transition at 10^{-8} M calmodulin implies that the binding constant is less than 10^{-9} M.

How can such data be used to calculate the fraction of the peptide that is free in solution (f_F) and the fraction bound to calmodulin (f_B)? The additivity law for anisotropies (eq. 10.6) is appropriate when f_i are the fractional intensities, not the fractional populations. Near 340 nm there is no change in intensity upon binding. If the polarized intensities are measured at this isoemissive point, the fraction of RS20 bound can be calculated using[50–51]

$$f_B = \frac{r - r_F}{r_B - r_F} \tag{10.50}$$

where r is the measured anisotropy, and r_F and r_B are the anisotropies of the free and bound peptides, respectively. The value of r_F is obtained by measuring the anisotropy of the free fluorophores, in this case the RS20 peptide prior to addition of calmodulin. The value of r_B is typically obtained from the limiting value observed when binding is thought to be complete. At different observation wavelengths the measured anisotropy can be weighted toward the free or bound forms. For instance, at 320 nm the bound peptide

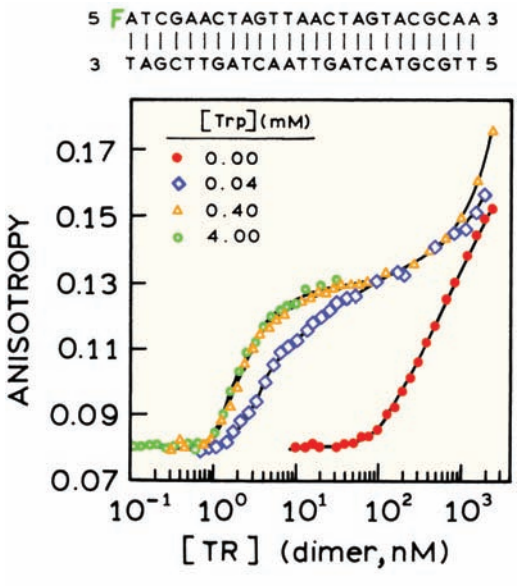

Figure 10.21. Anisotropy of the fluorescein (F)-labeled repressor DNA sequence upon titration with the Trp repressor (TR). Revised and reprinted with permission from [52]. Copyright © 1993, American Chemical Society.

contributes more strongly to the measured anisotropy. Under these conditions the fraction bound is given by

$$f_B = \frac{r - r_F}{(r - r_F) + R(r_B - r)} \qquad (10.51)$$

where $R = f_B/f_F$ is the ratio of intensities of the bound and free forms. Note that in eq. 10.51 the value of f_B represents the fractional concentration and not the fractional intensity. The fractional concentrations can be used to calculate the dissociation constant for the reaction.

10.7.2. Binding of the Trp Repressor to DNA

Studies of tryptophan repressor protein binding to DNA[52] are other examples of anisotropy measurements. In the presence of tryptophan this protein binds to several regions of the *E. coli* genome, one of which controls tryptophan synthesis. Binding to this region of the genome suppresses the transcription of genes for proteins that are in the tryptophan synthesis pathway. The trp repressor binds to the DNA sequence shown in Figure 10.21. This double-stranded sequence was labeled with fluorescein on one of its 5' ends. Upon addition of the repressor protein the fluorescein anisotropy increases due to the decreased rotational rate of the DNA 25-mer when bound to the repressor. The concentration of repressor needed for binding was strongly dependent on the concentration of tryptophan in solution. The binding to DNA was much stronger in the presence of tryptophan, which can be seen from the anisotropy increasing at lower TR concentrations. This is consistent with the known function of the repressor, which is to turn off the genes responsible for tryptophan synthesis when tryptophan levels are adequate.

The titration curves shown in Figure 10.21 can be understood in terms of a model of Trp repressor binding to DNA (Figure 10.22). Binding of tryptophan to the repressor increases the repressor affinity for DNA. This model also explains another feature of the titration curves, which is the further increase in anisotropy at higher repressor concentrations (Figure 10.21). Apparently, the DNA 25-mer can bind more than a single repressor dimer, and this additional binding occurs at higher repressor concentrations.

10.7.3. Helicase-Catalyzed DNA Unwinding

Anisotropy measurements are rather simple and can be made rapidly. This allows anisotropies to be used to study reaction kinetics occurring in fractions of a second.[53–55] One example is unwinding of double-helical DNA by helicase.[56] Helicases are found in all species from humans to bacteria. Unwinding of DNA is necessary for DNA replication. Helicases move along DNA in a single direction and destabilize the DNA base pairs using energy derived from ATP. The helicases typically prefer to act on oligomers that have a single-stranded region.

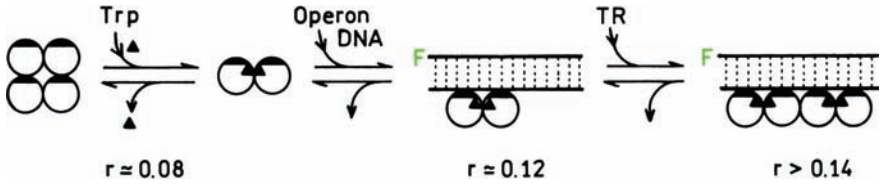

Figure 10.22. Binding of the Trp repressor to DNA. Revised and reprinted with permission from from [52]. Copyright © 1993, American Chemical Society.

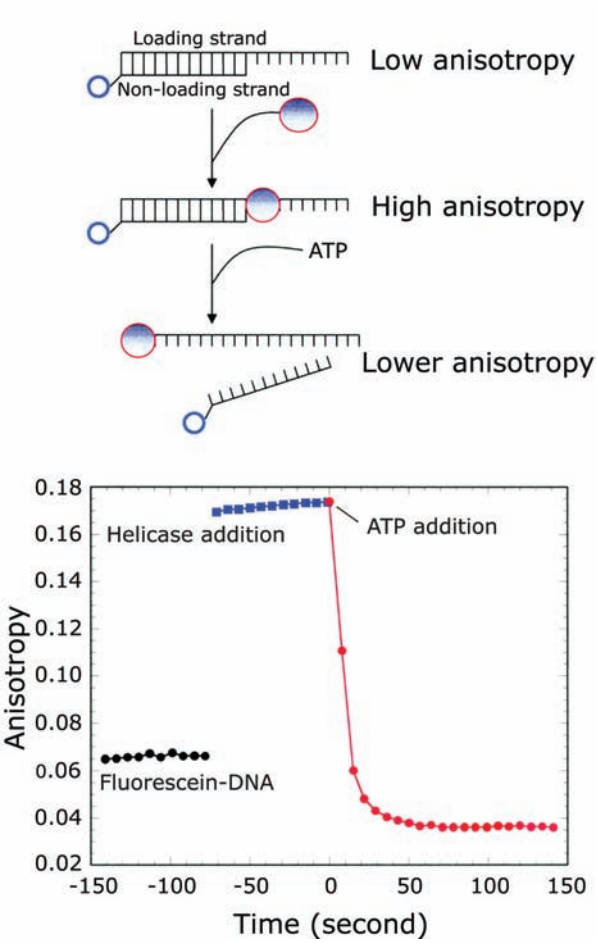

Figure 10.23. Effect of *E. coli*. helicase on a fluorescein-labeled DNA oligomer. Revised from [56].

Figure 10.23 shows anisotropy measurements of a fluorescein-labeled oligomer in the presence of helicase. The anisotropy increases immediately upon addition of helicase to the DNA, showing that the binding reaction occurs rapidly. The anisotropy then remains constant because there is no source of energy to disrupt the hydrogen bonded base pairs. Upon addition of ATP the anisotropy drops rapidly to a value lower than the starting value. The final anisotropy is lower because the labeled DNA strand is no longer bound to the complementary strand. The single-stranded oligomer has a lower molecular weight and is more flexible than the double-stranded oligomer. In this experiment the DNA strands did not reassociate during the experiment. This helicase will not rebind to DNA shorter than a 20-mer. These results show that anisotropy measurements can be used to follow the kinetics of biochemical reactions on a rapid timescale.

10.7.4. Melittin Association Detected from Homotransfer

In the preceding examples the binding reaction was detected from the increase in anisotropy resulting from the larger correlation time. Homo-resonance energy transfer can also be used to detect binding interactions. This is shown for melittin, which self-associates at high salt concentrations (Chapter 16). Melittin was randomly labeled with fluorescein isothiocyanate.[57] When the solution contained a small fraction of labeled melittin (1 of 25) the anisotropy increased at high salt concentrations (Figure 10.24). When all the melittin molecules were labeled, their anisotropy decreased markedly at high salt concentration. This decrease may be unexpected because melittin forms a tetramer in high salt solution, so its correlation time should increase fourfold. The decrease in anisotropy can be understood from the spectral properties of fluorescein (Chapter 3). The small Stokes shift and large overlap results in a Förster distance (R_0) of 53 Å for homotransfer. The anisotropy decrease in Figure 10.24 is due to homotransfer between fluoresceins in the melittin tetramer.

10.8. ANISOTROPY OF MEMBRANES AND MEMBRANE-BOUND PROTEINS

10.8.1. Membrane Microviscosity

Fluorescence anisotropy measurements can be used to study biological membranes. These studies have their origin

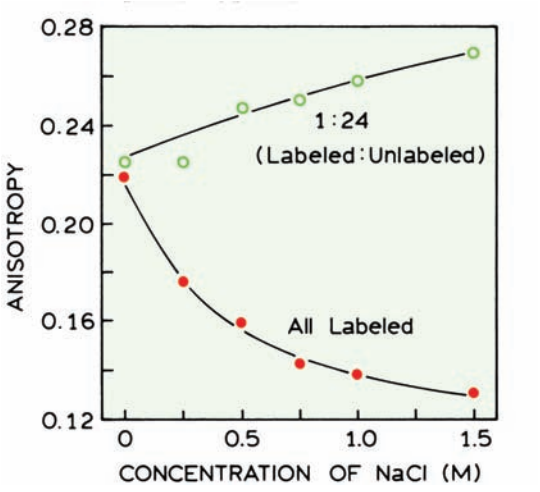

Figure 10.24. Self-association of melittin labeled with fluorescein in a 1:24 mixture with unlabeled melittin (○) or for all melittin labeled with fluorescein (●). Revised and reprinted with permission from [57]. Copyright © 1995, Biophysical Society.

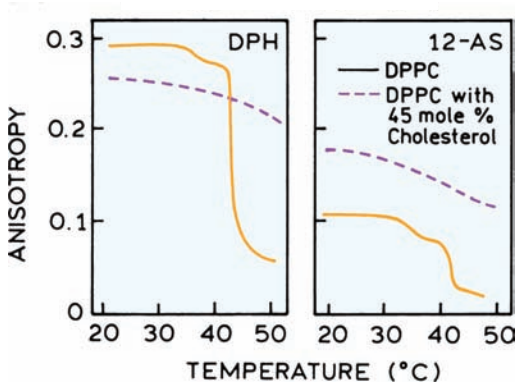

Figure 10.25. Temperature-dependent polarization of 12-anthroyloxy stearate and DPH in DPPC vesicles (solid), and in DPPC vesicles with 45 mole% cholesterol (dashed). Revised and reprinted from [61]. Copyright © 1982, with permission from Elsevier Science.

in the early studies of microviscosity of micelles and membranes.[58–60] The basic idea is to measure the anisotropy of a fluorophore in a reference solvent of known viscosity, and then in the membrane. The microviscosity of the membrane is then estimated by comparison with the viscosity calibration curve.

At present there is less use of the term "microviscosity" because fluorophores in membranes display complex anisotropy decays, which prevents a straightforward comparison of the solvent and membrane data (Chapter 11). However, steady-state and time-resolved anisotropies are still widely used because of the dramatic changes which occur at the membrane phase transition temperature. This is illustrated by the steady-state polarization of 12-anthroyloxy stearate (12-AS) and DPH in DPPC vesicles (Figure 10.25). For both 12-AS and DPH the polarization decreases at 37°C, which is the phase-transition temperature of DPPC. The change is more dramatic for DPH than for 12-AS, which is one reason why DPH is so widely used. The polarization values are sensitive to the presence of cholesterol, which tends to make the membranes more rigid and to eliminate the sharp phase transition. In the following chapter we will see that the anisotropy values may not reflect the rate of probe rotation in the membranes, but rather the extent to which the probe motions are restricted by the anisotropic membrane environment.

10.8.2. Distribution of Membrane-Bound Proteins

In a cuvette experiment it is possible to control the fluorophore concentration, so that changes in quantum yield can be detected. In fluorescence microscopy this is usually not possible because the local probe concentration is usually not known. Hence a high local intensity could be due to either a high probe concentration or a high quantum yield in this region of the cell. Anisotropy measurements are ratiometric and, in the absence of other effects, independent of the probe concentration. Hence, when observing a cell, the anisotropy can provide useful information even if the local probe concentration is not known.

In Figure 10.24 we saw how homotransfer could decrease the anisotropy of nearby fluorophores. This effect was used to search for clusters of membrane-bound proteins in CHO cells.[62] The protein of interest was a folate receptor (FR). The FR is present in two forms: FR-GPI is a form that binds to glycosylphosphatidylinositol (GPI), and FR-TM is a transmembrane form not thought to bind to GPI. There are a number of GPI anchored proteins that are thought to be involved in lateral segregation of proteins in membranes. However, such clusters or domains could not be observed using fluorescence microscopy, suggesting that they were smaller than the resolution of an optical microscope.

Optical resolution is usually limited to structures over 300 nm in size. RET occurs over much smaller distances, and should thus be able to detect clustering even if the clusters are below optical resolution. The experimental concept is shown in Figure 10.26. Suppose the labeled proteins are distributed randomly in the membrane (top), at a concentration large enough for RET to occur. If the fluorophore concentration is decreased the anisotropy will increase because of less homo-RET.

Now suppose the fluorophores are contained in small clusters (Figure 10.26, bottom). The clusters are assumed to be too small to be seen in a microscope. If the fluorophore concentration in the membrane deceases there is no change in the anisotropy because the fluorophores are still in clusters with the same proximity to each other. This schematic suggests formation of protein clusters in membranes can be detected from the anisotropy measurements.

The CHO cells containing the labeled folate receptors were imaged using fluorescence microscopy (Figure 10.27). The images were recorded through a polarizer oriented at 0 or 90° relative to the polarized excitation. The polarized intensity images were used to calculate a total intensity image using $I_{\parallel} + 2I_{\perp}$ (top panels). For both forms of the receptor there are regions of high and low intensity, suggesting variations in the receptor concentrations. However, domains were not detectable.

The intensity images were used to calculate the anisotropy images (Figure 10.27, lower panels). For FR-

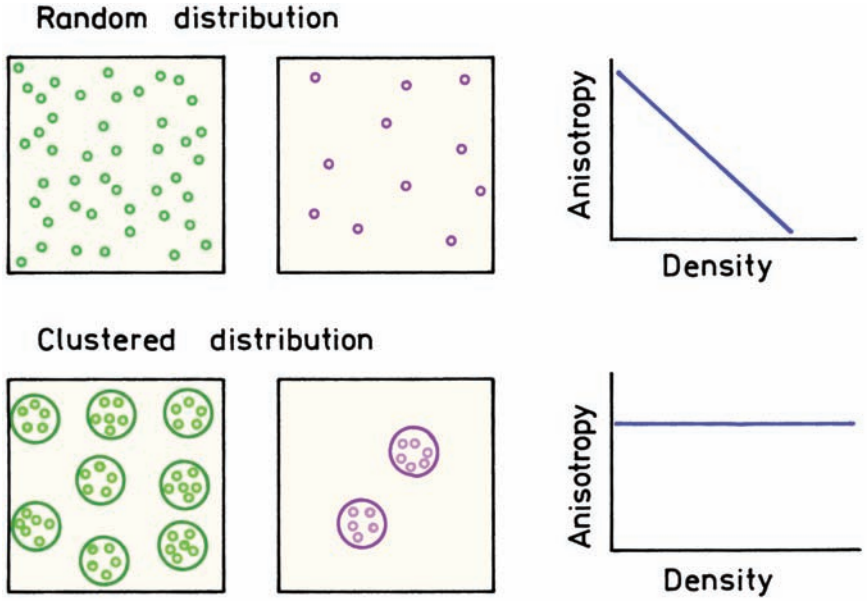

Figure 10.26. Effect of homotransfer on the anisotropy of a labeled membrane-bound protein for a random (top) and clustered (bottom) distribution. Revised from [62].

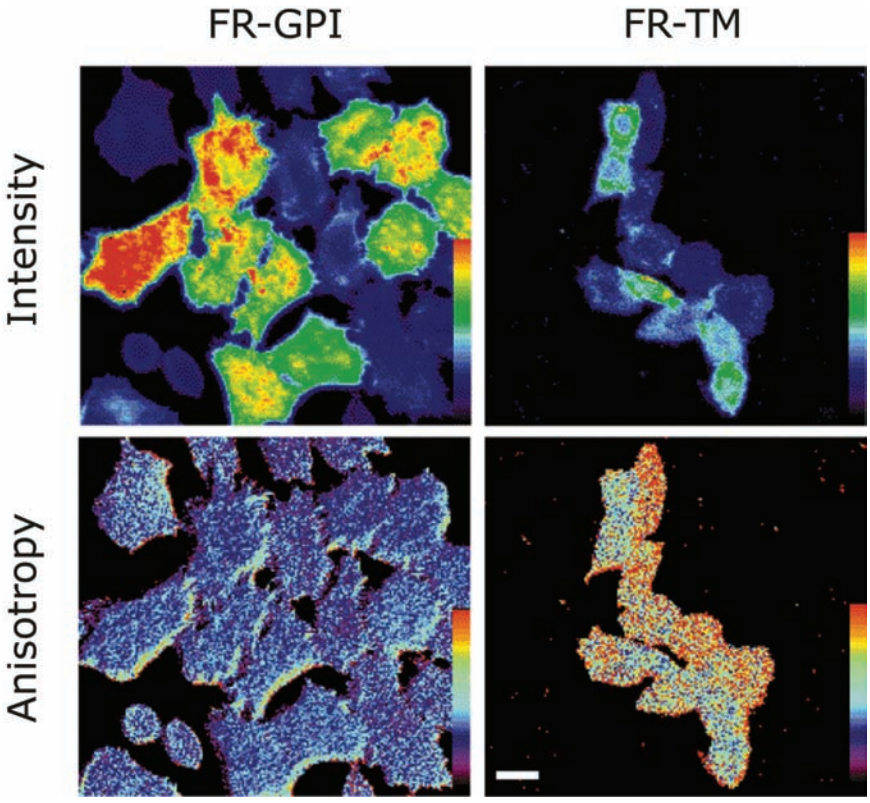

Figure 10.27. Intensity (top) and anisotropy image (bottom) of labeled folate receptors in CHO cells. Bar is 20 μm. Revised from [62].

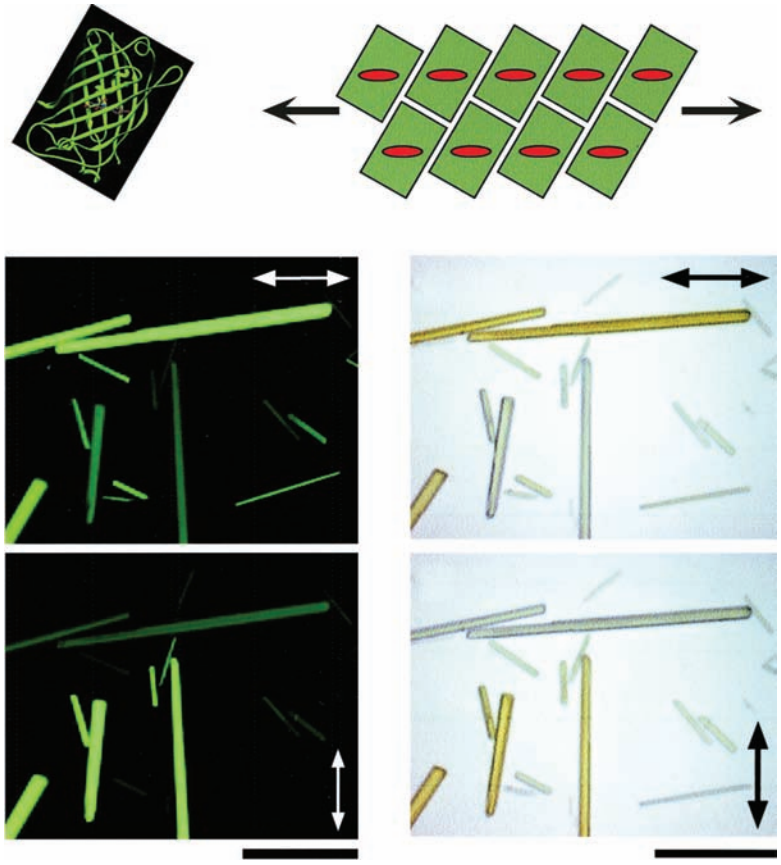

Figure 10.28. Transillumination fluorescence microscope image (left) and white light microscope image (right) of GFP crystals. The arrows indicate the direction of the direction of the incident polarization. The bars are 30 μm. The upper schematic shows the orientation of GFP (green) and the red shapes the orientation of the chromophore transition moment of the crystals. Revised from [64].

GPI, the anisotropy appears to be independent of the total intensity. For FR-TM the anisotropy is lower where the intensities are higher. FR-TM was not expected to form clusters. The decrease in anisotropy with increasing intensity (density) is consistent with the top panel in Figure 10.26 for randomly distributed proteins. FR-GPI was expected to exist in small clusters. The constant anisotropy independent of intensity (density) is consistent with the cluster model in the lower panel of Figure 10.26. These results show how the principles of anisotropy and RET are being extended to cellular imaging.

10.9. TRANSITION MOMENTS

The concept of a transition moment is somewhat abstract. When fluorophores are observed in random solutions the nonzero anisotropy values prove that the transition moments exist, but the data do not indicate the direction of the moment in the molecular structure. However, the direction of the transition moment can be determined if the fluorophores are oriented. A dramatic example[63–64] is shown for GFP in Figure 10.28. The left panels show microscopic images of the emission from GFP crystals. Depending on the orientation of the incident polarization the crystals are either bright or dark. This result shows that the chromophore in GFP is aligned along the long axis of the crystals. The orientation of GFP and its chromophore in the crystals is shown in the upper schematic. The β-barrel of GFP is oriented at an angle to the long axis, but the transition moments are aligned along the long axis.

Also shown in Figure 10.28 (right) are color images of the crystals when transilluminated with polarized white light. The crystals aligned with the incident polarization are yellow. The crystals are clear or very pale blue when rotated 90° from the incident polarization. This phenomenon is called dichroism. The yellow color is the result of the blue-light absorption of GFP that occurs primarily when the transition moments are aligned with the incident polarization.

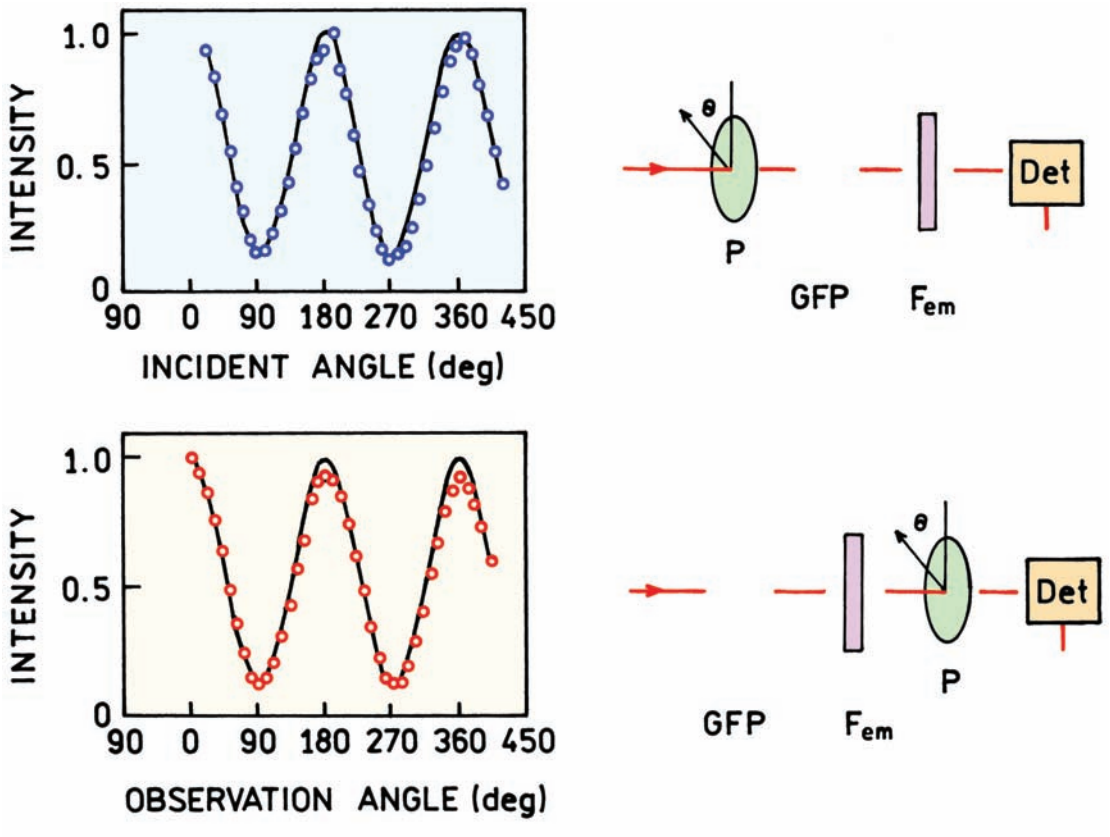

Figure 10.29. Fluorescence intensities of GFP crystals when illuminated with polarized light (top) or observed through a polarizer. For both traces only a single polarizer was used. Revised from [64].

Recall from Section 10.2 that for a random solution the maximum ratio of the polarized intensities was $I_{\parallel}/I_{\perp}$ = 3. Much greater contrast can be obtained with an oriented system. Figure 10.29 shows the intensities of the GFP crystals using a single polarizer for the excitation and observation without an emission polarizer (top). The intensity changed by a factor close to 10. This result is due to the $\cos^2 \theta$ photoselection of the absorption. The crystals only absorb when the transition moment is aligned with the incident polarization.

This experiment was repeated with unpolarized excitation and observation through an emission polarizer (Figure 10.29, bottom). A similar curve was observed, but for a different reason. In this case, the emission is almost completely polarized along the long axis of the crystal. The $\cos^2 \theta$ dependence is due to the transmission efficiency as the emission polarizer is rotated. It was not necessary to use polarized excitation because the oriented chromophores emit light polarized along their transition moment irrespective of the polarization of the incident light. Another important point from Figure 10.29 is that the absorption and emission transmission moments are nearly colinear. Otherwise there would be a shift in the phase of the two curves.

This example is instructive because it demonstrates several principles, in addition showing the existence and orientation of the transition moments. The chromophore in GFP is buried in the protein and held rigidly in a unique orientation. Otherwise the contrast ratio in Figure 10.29 would be smaller. Also, GFP shows a good Stokes shift and the protein separates the chromophores by a reasonable distance. If the chromophores were in direct contact there would probably be energy transfer, which could result in some depolarization.

REFERENCES

1. Jablonski A. 1960. On the notion of emission anisotropy. *Bull l'Acad Pol Sci, Ser A* **8**:259–264.
2. Weber G, 1952. Polarization of the fluorescence of macromolecules, I: theory and experimental method. *Biochem J* **51**:145–155.

3. Weber G, 1966. Polarization of the fluorescence of solutions. In *Fluorescence and phosphorescence analysis*, pp. 217–240. Ed DM Hercules. John Wiley & Sons, New York.
4. Selényi P. 1939. Wide-angle interferences and the nature of the elementary light sources. *Phys Rev* **56**:477–479.
5. Griffiths DJ. 1999. *Introduction to electrodynamics*. Prentice Hall, Englewood Cliffs, NJ.
6. Born M, Wolf E. 1980. *Principles of optics electromagnetic theory of propagation, interference and diffraction of light*. Pergamon Press, New York.
7. Lakowicz JR, Gryczynski I. 1997. Multiphoton excitation of biochemical fluorophores. In *Topics in fluorescence spectroscopy*, Vol. 5: *Nonlinear and two-photon induced fluorescence*, pp. 87–144. Ed JR Lakowicz. Plenum Press, New York.
8. Faucon JF, Lakowicz JR. 1987. Anisotropy decay of diphenylhexatriene in melittin-phospholipid complexes by multifrequency phase-modulation fluorometry. *Arch Biochem Biophys* **252**(1):245–258.
9. Herman P, Konopásek I, Plásek J, Svobodová J. 1994. Time-resolved polarized fluorescence studies of the temperature adaptation in *Bacillus subtilis* using DPH and TMA-DPH fluorescent probes. *Biochim Biophys Acta* **1190**:1–8.
10. Shinitzky M, Barenholz Y. 1974. Dynamics of the hydrocarbon layer in liposomes of lecithin and sphingomyelin containing dicetylphosphate. *J Biol Chem* **249**:2652–2657.
11. Thompson RB, Gryczynski I, Malicka J. 2002. Fluorescence polarization standards for high-throughput screening and imaging. *Biotechnology* **32**:34–42.
12. Michl J, Thulstrup EW. 1986. *Spectroscopy with polarized light*. VCH Publishers, New York.
13. Albinsson B, Kubista M, Nordén B, Thulstrup EW. 1989. Near-ultraviolet electronic transitions of the tryptophan chromophore: linear dichroism, fluorescence anisotropy, and magnetic circular dichroism spectra of some indole derivatives. *J Phys Chem* **93**:6646–6655.
14. Albinsson B, Eriksson S, Lyng R, Kubista M. 1991. The electronically excited states of 2-phenylindole. *Chem Phys* **151**:149–157.
15. Kubista M, Åkerman B, Albinsson B. 1989. Characterization of the electronic structure of 4',6-diamidino-2-phenylindole. *J Am Chem Soc* **111**:7031–7035.
16. Vincent M, de Foresta B, Gallay J, Alfsen A. 1982. Nanosecond fluorescence anisotropy decays of n-(9-anthroyloxy) fatty acids in dipalmitoylphosphatidylcholine vesicles with regard to isotropic solvents. *Biochemistry* **21**:708–716.
17. Mullaney JM, Thompson RB, Gryczynski Z, Black LW. 2000. Green fluorescent protein as a probe of rotational mobility within bacteriophage T4. *J Virol Methods* **88**:35–40.
18. Weber G. 1960. Fluorescence-polarization spectrum and electronic-energy transfer in tyrosine, tryptophan and related compounds. *Biochem J* **75**:335–345.
19. Valeur B, Weber G. 1977. Resolution of the fluorescence excitation spectrum of indole into the ^1L_a and ^1L_b excitation bands. *Photochem Photobiol* **25**:441–444.
20. Eftink MR, Selvidge LA, Callis PR, Rehms AA. 1990. Photophysics of indole derivatives: Experimental resolution of L_a and L_b transitions and comparison of theory. *J Phys Chem* **94**:3469–3479.
21. Shen X, Knutson JR. 2001. Subpicosecond fluorescence spectra of tryptophan in water. *J Phys Chem B* **105**:6260–6265.
22. Short KW, Callis PR. 2002. One- and two-photon spectra of jet-cooled 2,3-dimethylindole: ^1L_b and ^1L_a assignments. *Chem Phys* **283**: 269–278.
23. Yamamoto Y, Tanaka J. 1972. Polarized absorption spectra of crystals of indole and its related compounds. *Bull Chem Soc Jpn* 65:1362–1366.
24. Suwaiyan A, Zwarich R. 1987. Absorption spectra of substituted indoles in stretched polyethylene films. *Spectrochim Acta* **43A**(5): 605–609.
25. Weber G, Shinitzky M. 1970. Failure of energy transfer between identical aromatic molecules on excitation at the long wave edge of the absorption spectrum. *Proc Natl Acad Sci USA* **65**(4):823–830.
26. Kawski A. 1992. *Fotoluminescencja roztworów*. Wydawnictwo Naukowe PWN, Warsaw.
27. Van Der Meer BW, Coker III G, Chen S-YS. 1991. *Resonance energy transfer theory and data*. Wiley-VCH, New York.
28. Jablonski A. 1970. Anisotropy of fluorescence of molecules excited by excitation transfer. *Acta Phys Pol A* **38**:453–458.
29. Baumann J, Fayer MD. 1986. Excitation transfer in disordered two-dimensional and anisotropic three-dimensional systems: effects of spatial geometry on time-resolved observables. *J Chem Phys* **85**:4087–4107.
30. Teale FWJ. 1969. Fluorescence depolarization by light scattering in turbid solutions. *Photochem Photobiol* **10**:363–374.
31. Ghosh N, Majumder SK, Gupta PK. 2002. Fluorescence depolarization in a scattering medium: effect of size parameter of a scatterer. *Phys Rev E* **65**:026608-1–6.
32. Lentz BR. 1979. Light scattering effects in the measurement of membrane microviscosity with diphenylhexatriene. *Biophys J* **25**:489–494.
33. Berberan-Santos MN, Nunes Pereira EJ, Martinho JMG. 1995. Stochastic theory of molecular radiative transport. *J Chem Phys* **103**(8):3022–3028.
34. Nunes Pereira EJ, Berberan-Santos MN, Martinho JMG. 1996. Molecular radiative transport, II: Monte-Carlo simulation. *J Chem Phys* **104**(22):8950–8965.
35. Perrin F. 1929. La fluorescence des solutions: induction moleculaire. Polarisation et duree d'emission. Photochimie. *Ann Phys*, Ser 10 **12**:169–275.
36. Perrin F. 1926. Polarisation de la lumière de fluorescence: vie moyenne des molécules dans l'état excité. *J Phys Radium V*, Ser 6 **7**:390–401.
37. Perrin F. 1931. Fluorescence: durée élémentaire d'émission lumineuse. *Conférences D'Actualités Scientifiques et Industrielles* **22**:2–41.
38. Weber G. 1953. Rotational Brownian motion and polarization of the fluorescence of solutions. *Adv Protein Chem* **8**:415–459.
39. Yguerabide J, Epstein HF, Stryer L. 1970. Segmental flexibility in an antibody molecule. *J Mol Biol* **51**:573–590.
40. Weber G. 1952. Polarization of the fluorescence of macromolecules, II: fluorescence conjugates of ovalbumin and bovine serum albumin. *Biochem J* **51**:155–167.
41. Laurence DJR. 1952. A study of the absorption of dyes on bovine serum albumin by the method of polarization of fluorescence. *Biochem J* **51**:168–180.

42. Gottlieb YYa, Wahl Ph. 1963. Étude théorique de la polarisation de fluorescence des macromolecules portant un groupe émetteur mobile autour d'un axe de rotation. *J Chim Phys* **60**:849–856.
43. Ferguson BQ, Yang DCH. 1986. Methionyl-tRNA synthetase induced 3'-terminal and delocalized conformational transition in $tRNA^{fMet}$: steady-state fluorescence of tRNA with a single fluorophore. *Biochemistry* **25**:529–539.
44. Buchner J. 1996. Supervising the fold: functional principals of molecular chaperones. *FASEB J* **10**:10–19.
45. Ellis RJ. 1996. *The chaperonins*. Academic Press, New York.
46. Braig K, Otwinowski Z, Hegde R, Bolsvert DC, Joachimiak A, Horwich AL, Sigler PB. 1994. The crystal structure of the bacterial chaperonin GroEL at 2.8 Å. *Nature* **371**:578–586.
47. Gorovits BM, Horowitz PM. 1995. The molecular chaperonin cpn60 displays local flexibility that is reduced after binding with an unfolded protein. *J Biol Chem* **270**(22):13057–13062.
48. Lim K, Jameson DM, Gentry CA, Herron JN. 1995. Molecular dynamics of the anti-fluorescein 4-4-20 antigen-binding fragment, 2: time-resolved fluorescence spectroscopy. *Biochemistry* **34**:6975–6984.
49. Lukas TJ, Burgess WH, Prendergast FG, Lau W, Watterson DM. 1986. Calmodulin binding domains: characterization of a phosphorylation and calmodulin binding site from myosin light chain kinase. *Biochemistry* **25**:1458–1464.
50. Malencik DA, Anderson SR. 1984. Peptide binding by calmodulin and its proteolytic fragments and by troponin C. *Biochemistry* **23**:2420–2428.
51. Eftink MR, 1994. The use of fluorescence methods to monitor unfolding transitions in proteins. *Biophys J* **66**:482–501.
52. LeTilly V, Royer CA. 1993. Fluorescence anisotropy assays implicate protein–protein interactions in regulating *trp* repressor DNA binding. *Biochemistry* **32**:7753–7758.
53. Banik U, Beechem JM, Klebanow E, Schroeder S, Weil PA. 2001. Fluorescence-based analyses of the effects of full-length recombinant TAF130p on the interaction of TATA box-binding protein with TATA box DNA. *J Biol Chem* **276**(52):49100–49109.
54. Hiller DA, Fogg JM, Martin AM, Beechem JM, Reich NO, Perona JJ. 2003. Simultaneous DNA binding and bending by ecoRV endonuclease observed by real-time fluorescence. *Biochemistry* **42**:14375–14385.
55. Taniguchi M, Yoshimi T, Hongo K, Mizobata T, Kawata Y. 2004. Stopped-flow fluorescence analysis of the conformational changes in the GroEL apical domain. *J Biol Chem* **279**(16):16368–16376.
56. Xu HQ, Zhang AH, Auclair C, Xi XG. 2003. Simultaneously monitoring DNA binding and helicase-catalyzed DNA unwinding by fluorescence polarization. *Nucleic Acids Res* **31**(14):e70.
57. Runnels LW, Scarlata SF. 1995. Theory and application of fluorescence homotransfer to melittin oligomerization. *Biophys J* **69**:1569–1583.
58. Shinitky M, Dianoux AC, Gitler C, Weber G. 1971. Microviscosity and order in the hydrocarbon region of micelles and membranes determined with fluorescence probes, I: synthetic micelles. *Biochemistry* **10**:2106–2113.
59. Cogen U, Shinitzky M, Weber G, Nishida T. 1973. Microviscosity and order in the hydrocarbon region of phospholipid and phospholipid–cholesterol dispersions determined with fluorescent probes. *Biochemistry* **12**:521–528.
60. Thulborn KR, Tilley LM, Sawyer WH, Treloar FE. 1979. The use of n-(9-anthroyloxy) fatty acids to determine fluidity and polarity gradients in phospholipids bilayers. *Biochim Biophys Acta* **558**:166–178.
61. Thulborn KR, Beddard GS. 1982. The effects of cholesterol on the time-resolved emission anisotropy of 12-(9-anthroyloxy)stearic acid in dipalmitoylphosphatidylcholine bilayers. *Biochim Biophy Acta* **693**:246–252.
62. Varma R, Mayor S. 1998. GPI-anchored proteins are organized in submicron domains at the cell surface. *Nature* **394**:798–801.
63. Rosell FI, Boxer SG. 2003. Polarized absorption spectra of green fluorescent protein single crystals: transition dipole moment directions. *Biochemistry* **42**:177–183.
64. Inoué S, Shimomura O, Goda M, Shribak M, Tran PT. 2002. Fluorescence polarization of green fluorescence protein. *Proc Natl Acad Sci USA* **99**(7):4272–4277.

ADDITIONAL READING ON THE APPLICATION OF ANISOTROPY

Association Reactions

Hey T, Lipps G, Krauss G. 2001. Binding of XPA and RPA to damaged DNA investigated by fluorescence anisotropy. *Biochemistry* **40**:2901–2910.

Imaging

Lidke DS, Nagy P, Barisas BG, Heintzmann R, Post JN, Lidke KA, Clayton AHA, Arndt-Jovin DJ, Jovin TM. 2003. Imaging molecular interactions in cells by dynamic and static fluorescence anisotropy (rFLIM and emFRET). *Biochem Soc Trans* **31**(5):1020–1027.

Membranes

Gidwani A, Holowka D, Baird B. 2001. Fluorescence anisotropy measurements of lipid order in plasma membranes and lipid rafts from RBL-2H3 mast cells. *Biochemistry* **40**:12422–12429.

Huertas ML, Cruz V, Cascales JJ, Acuña AU, Garcia de la Torre J. 1996. Distribution and diffusivity of a hydrophobic probe molecule in the interior of a membrane: theory and simulation. *Biophys J* **71**:1428–1439.

Sinha M, Mishra S, Joshi PG. 2003. Liquid-ordered microdomains in lipid rafts and plasma membrane of U-87 MG cells: a time-resolved fluorescence study. *Eur Biophys J* **32**:381–391.

Oriented Systems

Fisz JJ, Buczkowski M. 2001. Excited-state orientation-dependent irreversible interconversion and fluorescence depolarization in organized molecular media, I: theory. *J Chem Phys* **115**(15):7051–7060.

Dale RE, Hopkins SC, an der Heide UA, Marszalek T, Irving M, Goldman YE. 1999. Model-independent analysis of the operation of fluorescent probes with restricted mobility in muscle fibers. *Biophys J* **76**:1606–1618.

RET and Anisotropy

Andrews DL, Juzeliunas G. 1991. The range dependence of fluorescence anisotropy in molecular energy transfer. *J Chem Phys* **95**(8): 5513–5518.

Cohen-Kashi M, Moshkov S, Zurgil N, Deutsch M. 2002. Fluorescence resonance energy transfers measurements on cell surfaces via fluorescence polarization. *Biophys J* **83**:1395–1402.

Gaab KM, Bardeen CJ. 2004. Wavelength and temperature dependence of the femtosecond pump-probe anisotropies in the conjugated polymer MEH-PPV: implications for energy-transfer dynamics. *J Phys Chem B* **108**:4619–4626.

Kleima FJ, Hofmann E, Gobets B, van Stokkum IHM, van Grondelle R, Diederichs K, van Amerongen H. 2000. Förster excitation energy transfer in peridinin-chlorophyll-*a*-protein. *Biophys J* **78**:344–353.

Tanaka F. 1998. Theory of time-resolved fluorescence under the interaction of energy transfer in bichromophoric system: effect of internal rotations of energy donor and acceptor. *J Chem Phys* **109**(3):1084–1092.

Varnavski OP, Ostrowski J, Bazan GC, Goodson III T. 2002. Energy transfer and fluorescence depolarization in organic dendrimers and branched molecules. *Proc SPIE* **4464**:134–141.

Surfaces

Ishizaka S, Kinoshita S, Nishijima Y, Kitamura N. 2003. Direct observation of molecular recognition mediated by triple hydrogen bonds at a water/oil interface: time-resolved total internal reflection fluorometry study. *Anal Chem* **75**(22):6035–6042.

Theory

Bajzer Z, Moncrieffe MC, Penzar I, Prendergast FG. 2001. Complex homogeneous and heterogeneous fluorescence anisotropy decays: enhancing analysis accuracy. *Biophys J* **81**:1765–1775.

Bialik CN, Wolf B, Rachofsky EL, Alexander Ross JB, Laws WR. 1998. Dynamics of biomolecules: assignment of local motions by fluorescence anisotropy decay. *Biophys J* **75**:2564–2573.

Bryant J, Bain AJ. 1998. Controlled orientational photoselection via three-pulse excitation. *Chem Phys Lett* **286**:121–130.

Fisz JJ. 1998. Flexible fluorophores as the probes for monitoring the structural and dynamical properties of organized molecular media. *Chem Phys Lett* **297**:409–418.

Fisz JJ. 1996. Polarized fluorescence spectroscopy of two-ground- and two-excited-state systems in solutions. *Chem Phys Lett* **262**:495–506.

Tanaka F. 2000. Effects of internal rotations on the time-resolved fluorescence in a bichromophoric protein system under the energy transfer interaction. *J Fluoresc* **10**(1):13–19.

Tanaka F, Mataga N. 1998. Analytical theory of time-resolved fluorescence anisotropy and dynamic Stokes shift of polar solute molecules based on continuum model for solvent. *Chem Phys* **236**:277–289.

PROBLEMS

P10.1. *Angles (β) between Absorption and Emission Transition Moments*: Figure 12.34 shows the excitation anisotropy spectrum of perylene in propylene glycol at –60°C. What is the angle between the transition moments for excitation at 430, 290, and 270 nm?

P10.2. *Effect of Scattered Light in the Anisotropy*: Suppose a membrane-bound fluorophore displays a true anisotropy of 0.30. However, your emission filters allow 20% of the signal to be due to scattered light. What is the measured anisotropy?

P10.3. *Calculation of an Anisotropy*: Using a T-format polarization instrument you obtain the following data for diphenylhexatriene (DPH). The first and second subscripts refer to the orientation of the excitation and emission polarizers, respectively. Calculate r_0 and P_0 for DPH. What is the angle α between the absorption and emission oscillators?

Conditions	I_{HV}	I_{VV}
–60°C in propylene glycol	0.450	1.330

P10.4. *Derivation of the Perrin Equation*: Derive the Perrin equation (eq. 10.44) for a single-exponential decay of the intensity and anisotropy.

P10.5. *Calculation of an Anisotropy in Fluid Solution*: Calculate the expected anisotropy of perylene in ethanol at 20°C, and in propylene glycol at 25°C. The molecular weight of perylene is 252 g/mol, and the density can be taken as 1.35 g/ml. The viscosity of ethanol at 20°C is 1.194 cP, and that of propylene glycol at 25°C is 32 cP. Assume the lifetime is 6 ns, and $r_0 = 0.36$.

P10.6. *Binding Reactions by Anisotropy*: Derive eqs. 10.50 and 10.51, which describe the fractional binding from the steady-state anisotropy and the change in intensity on binding.

P10.7. *Calculation of a Binding Constant From Anisotropies*: Assume the probe 1-dimethylamino-5-naphthalene sulfonic acid (DNS) binds to bovine serum albumin (BSA). The DNS polarization values are given in Table 10.6. The dissociation constant (K_d) for the binding is given by

$$K_d = \frac{[\text{DNS}][\text{BSA}]}{[\text{DNS} - \text{BSA}]} \tag{10.52}$$

A. Calculate the dissociation constant assuming that the quantum yield of the probe is not altered upon binding.

B. Now assume that the quantum yield of DNS increases twofold upon binding to BSA. What is K_d?
C. How would you determine whether the quantum yield of DNS changes upon binding to BSA?
D. Predict the time-resolved anisotropies for each solution at 20°C. Assume $P_0 = 0.3913$ for DNS and that the rotational correlation times of DNS and BSA are well approximated by that predicted for an anhydrous sphere. The molecular weight of BSA is near 66,000 g/mol. The viscosity of water at 25°C is 0.894 cP (g cm^{-1} sec^{-1}). The density of BSA can be taken as 1.2 g/cm^3.

Table 10.6. Polarization Values of DNS

[BSA]	[DNS]	*P*
0	1 x 10^{-7} M	0.0149
2 x 10^{-5} M	1 x 10^{-7} M	0.2727
$>>K_d$	1 x 10^{-7} M	0.3913